metals

MDPI

Review

The Corrosion Behavior in Different Environments of Austenitic Stainless Steels Subjected to Thermochemical Surface Treatments at Low Temperatures: An Overview

Francesca Borgioli

Department of Industrial Engineering, University of Florence, via S. Marta 3, 50139 Florence, Italy; francesca.borgioli@unifi.it; Tel.: +39-055-275-8734

Abstract: Low-temperature thermochemical treatments are particularly suitable for use in the surface hardening of austenitic stainless steels without impairing their corrosion resistance. In fact, when using treatment media rich in nitrogen and/or carbon at relatively low temperatures (<450 °C for nitriding, <550 °C for carburizing), it is possible to inhibit the formation of chromium compounds and obtain modified surface layers that consist mainly of a supersaturated solid solution, known as expanded austenite or S-phase. It has been observed that this hard phase allows the enhancement of corrosion resistance in chloride-ion-containing solutions, while the results were contradictory for chloride-free acidic solutions. This overview aims to discuss the corrosion behavior of low-temperature-treated austenitic stainless steels, taking into account the different microstructures and phase compositions of the modified layers, as well as the different test environments and conditions. In particular, the corrosion behavior in both chloride-ion-containing solutions and chloride-free solutions (sulfuric acid, sulfate and borate solutions) is discussed. The analysis of the international literature presents evidence that the microstructure and phase composition of the modified layers have key roles in corrosion resistance, especially in sulfuric acid solutions.

Keywords: stainless steels; low-temperature treatments; nitriding; carburizing; expanded austenite; S-phase; corrosion resistance

check for updates

Citation: Borgioli, F. The Corrosion Behavior in Different Environments of Austenitic Stainless Steels Subjected to Thermochemical Surface Treatments at Low Temperatures: An Overview. *Metals* **2023**, *13*, 776. https://doi.org/10.3390/met13040776

Academic Editors: Nong Gao and Frank Czerwinski

Received: 28 February 2023
Revised: 30 March 2023
Accepted: 13 April 2023
Published: 15 April 2023

1. Introduction

Stainless steels owe their name to their capability to remain without apparent stain, i.e., without rust traces, in many environments due to their excellent resistance to general corrosion. The key element allowing to improve the corrosion resistance of these iron (Fe)-based alloys is chromium (Cr). Since the 19th century, it has been noted that Fe-Cr alloys have higher corrosion resistance in various environments in comparison with carbon steels, and that this resistance increases as the Cr content grows. However, the discovery of the first alloys, which nowadays are called stainless steels, can be dated to the period of 1905–1912 [1]. In stainless steels, Cr, added in a content of at least 10.5 wt.%, promotes the formation of a passive surface film. This is compact, adherent and self-healing if broken in the presence of oxygen, and it protects the substrate from corrosive environments [2,3]. Even if Cr oxide plays a fundamental role in the passive film, the structure and composition of the film are fairly complex and depend on the alloy elements of the stainless steel [4,5] and the conditions in which the film forms (for example, in air, in passivating solutions, with electrochemical treatments) [5–7]. Additionally, they may change when the steel is put in contact with the corrosive environment [8,9]. Therefore, the conditions over which passivity is maintained depend on both the stainless steel itself (composition, surface finishing) and the environment [3]. The passive behavior allows stainless steels to have very low rates of uniform corrosion in many environments [3,10]. The protective effect of the passive film may cease when the environment is too aggressive to allow for the maintenance of passivity. This fact occurs when the environment is too reducing, meaning

that the formation of passive species is inhibited (dissolution of the film in the active state), or too oxidizing, with the result that the oxidized species become not stable (transpassive dissolution of the film) [3,10]. As a consequence, general (uniform) corrosion may be observed when the alloys are put in contact with aqueous solutions of acids as hydrochloric acid (HCl) or sulfuric acid (H_2SO_4). Furthermore, the passive film may be locally broken and not able to reform, as occurs when halide ions are present or the sensitization of the steel occurs, and therefore localized corrosion phenomena are produced as pitting, crevices and intergranular corrosion [3,4,10]. Pitting and crevice corrosion can be particularly harmful since, even if the weight loss caused is usually negligible, corrosion may penetrate deeply into a steel component, prejudicing its structural integrity. Chloride-ions (Cl^-) are the most common causes of pitting attack due to their role in weakening the stability of passive films and decreasing their protective effect [3,10–12]. The combination of a Cl^- environment and tensile stress may also cause stress corrosion cracking phenomena [3,10]. Intergranular corrosion usually occurs when Cr compounds, as Cr carbides, precipitate at grain boundaries as a consequence of a thermal treatment, an event which causes so-called sensitization. The regions adjacent to the precipitate are depleted in Cr up to values lower than the passivity limit, and they become susceptible to corrosion phenomena at grain boundaries in aggressive environments [3,10].

Besides Cr, which stabilizes the body-centered cubic (b.c.c.) structure of α-Fe, or ferrite, other alloy elements may be added to steel. These include molybdenum (Mo), silicon (Si), niobium (Nb) and titanium (Ti), which are all ferrite-stabilizers, as well as nickel (Ni), manganese (Mn), carbon (C) and nitrogen (N), that stabilize the face-centered cubic (f.c.c.) structure of γ-Fe, austenite [2]. As a consequence, ferrite, austenite and martensite lattices and their related microstructures can be obtained, and the stainless steels are usually classified on the basis of these microstructures: ferritic, austenitic, martensitic, duplex (ferritic-austenitic) and precipitation hardening [2]. As recalled previously, alloy elements influence not only the mechanical properties and the workability of the different grades, but also the chemical composition, stability and thickness of the passive film, and hence the corrosion resistance [4].

Stainless steels are employed in many fields, from mild environments, such as for architectural applications, furniture and kitchenware, to the more severe ones, as components for chemical and power engineering industries [2,3,10]. Among the different steel grades, austenitic stainless steels have high corrosion resistance. This has resulted in them becoming the material of choice for many applications as components obtained by both conventional manufacturing techniques and additive manufacturing processes [10,13]. The use of these alloys can be extended further by improving their low surface hardness, poor tribological properties or their resistance to localized corrosion. Among the different surface engineering strategies, in the last years there has been an increasing interest in the so-called low-temperature thermochemical treatments, that have been the subjects of intensive research. Nitriding, carburizing or nitrocarburizing processes, which are usually applied to low-alloy steels or tool steels in order to obtain a N and/or C surface alloying by means of diffusion, cannot be transferred directly to stainless steels. In fact, when the same temperatures employed for the nitriding (500–550 °C) [14] or carburizing (850–980 °C) [14] of low-alloy steels and tool steels are used for stainless steels, Cr forms hard compounds (nitrides, carbides); therefore, the Cr-depleted matrix cannot maintain a uniform and protective passive film, and corrosion can easily occur [4,15]. However, by using temperatures so low that interstitial atoms (N, C) can easily diffuse while significant Cr (substitutional) diffusion cannot occur, the formation of Cr compounds is inhibited. In these so-called para-equilibrium conditions [16], N and C atoms are retained in solid solution in austenite lattice above the solubility limit and thus a supersaturated solid solution, known as "expanded austenite", forms.

The formation of modified surface layers consisting mainly of expanded austenite is known to increase surface hardness, improve tribological properties and enhance fatigue resistance. Regarding corrosion behavior, it has been reported that the modified layers

allow to maintain or even increase the corrosion resistance of austenitic stainless steels in Cl^--containing solutions. On the contrary, the studies on the corrosion resistance of low-temperature-treated austenitic stainless steels in Cl-free aqueous environments, such as sulfuric acid solutions, have given contradictory results. Low-temperature treatments have not only been performed on massive specimens, but also on coatings obtained with various techniques [17–19]. Recently, they have also been performed on powders that potentially are usable for thermal spraying and additive manufacturing [20,21]. From the first studies of the 1980s up to today, more than 1000 papers have been published on low-temperature treatments of stainless steels, with most of them concerning the treatment of austenitic stainless steels. Likewise, extended reviews [22–26] and briefs overviews have been produced on general [27–29] or on specific topics [30–32] regarded this steel grade, which has also been discussed in reviews regarding all the different stainless steel grades [33–35]. Although the effects of low-temperature treatments on the corrosion behavior of austenitic stainless steels are of paramount importance for the usability of these alloys and are the subjects of many studies, this topic has usually only been reported as a part of general reviews [22,24–27,33,36], being discussed without an in-depth analysis of the various factors which contribute to causing the success or the failure of the modified surface layers in a potential corrosive environment.

The aim of the present review is to report on and discuss the major studies on the characteristics of low-temperature-treated austenitic stainless steels and their corrosion behavior in different environments, in order to highlight the conditions which allow to maintain or even improve the corrosion resistance of the parent alloys. The review is organized into two main sections. The first section is devoted to discussing the solid solution of interstitial atoms in Fe and the formation of expanded austenite, as well as the effects of N and C on the passive film and corrosion resistance. The second section considers the characteristics of the modified surface layers which are formed in austenitic stainless steels and summarizes the corrosion behavior studies carried out in aqueous environments with and without Cl^- using different test conditions and methodologies, including electrochemical impedance spectroscopy (EIS) analysis, potentiodynamic and cyclic potentiodynamic polarization tests, galvanostatic tests, and immersion tests.

2. N and C Alloying of Fe and Its Effects on Corrosion Behavior

2.1. Interstitial Solid Solutions in Fe and Formation of Expanded Austenite

N and C atoms in Fe-based solid solutions are very effective strengtheners. In f.c.c. austenite interstitial solute atoms are usually accommodated in the larger octahedral sites (Figure 1a). According to Fe-N and Fe-C phase diagrams, the maximum solubility of N in f.c.c. γ-Fe is 10.3 at.% at 650 °C [37], while the maximum solubility of C is 9.23 at.% at 1147 °C [38].

Figure 1. Sketch of the f.c.c. lattice with the octahedral interstitial sites (red spheres) (**a**) and the tetrahedral interstitial sites (black spheres) (**b**).

The atomic radius of N is smaller than that of C, but the effective atom size of N in solid solutions is larger due to the influence on the density of electronic states at the Fermi level, which results in the f.c.c. lattice having larger distortion [39]. Moreover, in Fe-N

solid solutions, a tendency of short-range ordering of N atoms is observed; conversely, in Fe-C solid solutions there is a tendency towards the clustering of C atoms [39]. In stainless steels, the precipitation of Cr carbides, which causes the so-called sensitization, is fairly easy and can be considered to be a consequence of the clustering of C atoms and the C-assisted clustering of Cr atoms. Instead, N atoms tend to hinder the clustering of Cr atoms and precipitation of Cr nitrides and shift the sensitization curve in the time-temperature-transformation diagram to the right of the time scale. As a consequence, in an austenitic stainless steel such as AISI 316, the C content is maintained at a level lower than 0.015 at.% to avoid carbide precipitation [40], while the equilibrium solubility of N in austenite is larger, being less than 0.65 at.% [22].

When low-temperature thermochemical treatments are carried out, the (interstitial) diffusion of N and C is several orders of magnitude higher than that of substitutional atoms (Cr, Mn, Mo, Ni) that remain fairly "immobile" in the lattice [41]. Thus, the formation of nitrides or carbides tends to be inhibited, even if it should be favored from a thermodynamic point of view, and the interstitial atoms are retained in solid solution with a content that can be up to several hundred times higher than the level of equilibrium solubility, producing the so-called "colossal" supersaturation [40,42]. As a consequence, a significant lattice expansion of the original Fe-based lattice is observed, and this is particularly high when N is solubilized due to the fact that up to about 0.61 occupancy of the octahedral interstitial sites (equivalent to the number of interstitial atoms per metal atom in a f.c.c. lattice) may be obtained [23]. As the N content increases, it does not become clear whether the N atoms are hosted only in the octahedral sites (Figure 1a), so that there is a tendency to a more ordered structure as the NaCl-type structure of γ'''-FeN, or if the tetrahedral sites are also occupied (Figure 1b), so that the ZnS type of γ''-FeN tends to be produced [33]. In austenitic stainless steels, a maximum N content of ~38 at.% [42] is observed in the so-called N-rich expanded austenite, while the maximum C content in C-rich expanded austenite is ~19 at.% [43].

2.2. Effects of N and C on the Characteristics of the Passive Film

As mentioned before, the passive film has a key role in allowing the very good corrosion resistance of stainless steels in many environments owing to its capability of slowing corrosion (dissolution) reactions by many orders of magnitude. However, once formed, the passive film cannot be considered as a rigid layer, but rather a dynamic system capable of adjusting its composition and thickness as a consequence of the change in environmental conditions [44].

The passive film is enriched in Cr(III) oxide [8,45–47], but the amount depends on the passivation conditions. As recently summarized by Maurice and Marcus [47], the dissolution rate of Cr(III) oxide is smaller than that of Fe(II)/Fe(III) oxides in acid aqueous environments, meaning that a strong Cr enrichment occurs in the passive range. In the transpassive range, Cr dissolves as Cr(VI), decreasing the Cr content. In alkaline solutions, Fe(II)/Fe(III) oxides are less soluble, and Cr enrichment in the passive film decreases. The thickness of the passive film is typically about 1–3 nm [8,47].

In situ and ex situ analysis of the passive film points out that it has usually a complex structure. The outer region, at the film–electrolyte interface, is rich in Fe oxides and hydroxides, and the inner region, in contact with the metallic substrate, is rich in Cr oxide [45,46,48] (Figure 2a).

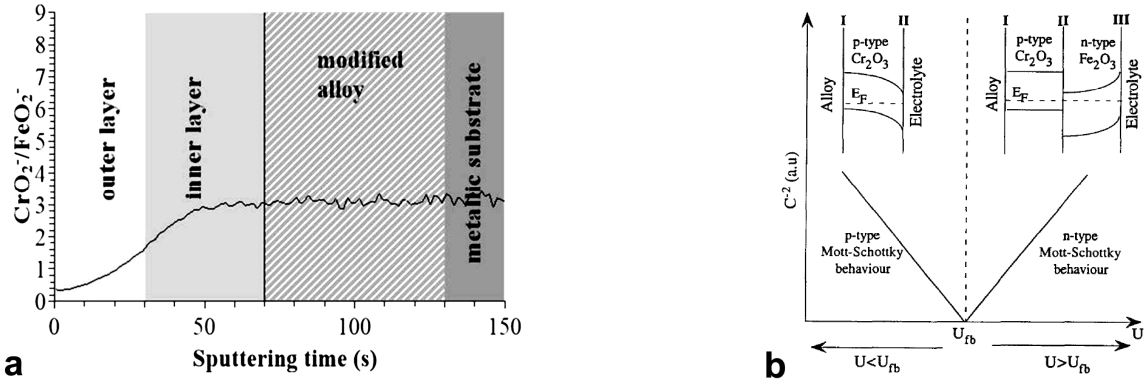

Figure 2. (**a**) CrO_2^- to FeO_2^- ratio in an air grown passive film (For further details, see Ref. [45]) (Reprinted from [45]. Reproduced under the terms of the CC-BY license. Copyright © 2019 Wang, Paschalidou, Seyeux, Zanna, Maurice and Marcus. Published by Frontiers Media S.A.). (**b**) Mott–Schottky plot and schematic representation of the electronic structure model of passive film (For further details, see Ref. [46]) (Reprinted with permission from Ref. [46]. Copyright 1995 Elsevier).

Surface alloying with N and/or C does not significantly change the structure of the passive film. However, these interstitial atoms remain "entrapped" in the film and contribute to the mitigation of corrosion phenomena. When N-rich expanded austenite (treated steel: 1Cr18Ni9Ti) is put in contact with a 3 wt.% NaCl solution, the passive film has an outer region rich in Fe hydroxide/oxide, which also has minor N content, and an inner Cr-rich hydroxide/oxide region in which N significantly increases, as can be detected by Auger electron spectroscopy (AES) and X-ray photoelectron spectroscopy (XPS) [49]. A similar structure, with an outer part enriched in Fe and the inner part enriched in Cr together with N, is observed when the passive layer formed in a borate buffer solution [50,51]. XPS analysis shows the presence of Cr-N and Fe-N bonds within the passive layer [49,50], and it is hypothesized that they are related to an $(Fe,Cr)_3(N,O)_4$ spinel present in the inner part of the passive layer [51]. High-resolution transmission electron microscopy (TEM) studies of the passive film, which forms on N-rich expanded austenite in a borate buffer solution, show that the film evolves when in contact with the solution. In particular, there is a change in the composition of the passive layer, and an increase in Cr and N content in the inner part of the film is observed after 3 h [51].

The analysis of passive films forming on C-rich expanded austenite by means of grazing incidence XPS shows that the film maintains a similar structure, with an inner layer rich in Cr-oxides and an outer layer in which comparable amounts of Fe and Cr are present [52]. Regarding C, a very high C content is detected at the surface, which is probably due to carbon soot, carbon contamination and carbon presence in the oxide film. At about 0.5 nm depth, C concentration markedly decreases after which it increases in the inner part of the passive film.

The passive films of stainless steels have semiconducting properties as their oxide layers are nonstoichiometric. By using Mott–Schottky analysis, it is observed that the outer Fe-rich oxide region has an *n*-type semiconductivity, while the inner Cr-rich oxide region has a *p*-type semiconductivity [46]. The *n*-type semiconductivity, caused by the presence of oxides such as Fe_2O_3, α, β and γ FeO(OH), MoO_3, is developed either by transport through interstitial diffusion or by anion diffusion inward toward the metal. Conversely, the *p*-type semiconductive behavior, caused by the presence of oxides such as Cr_2O_3, $FeCr_2O_4$, MoO_2, occurs owing to a deficiency in metal ions or excess of cation vacancies [53] (Figure 2b).

The N alloying influences this semiconductive behavior, and a decrease in donor and acceptor density is observed in AISI 316LN steel as the N content increases [53]. When a larger N content is present, such as for N-rich expanded austenite, a further significant reduction in the donor and acceptor density, up to about two orders of magnitude, is registered and a decrease in flat band potential, at which the transition from a *p*-type

into an *n*-type semiconductive behavior occurs, is reported [50,54]. A similar effect is observed for C-rich expanded austenite, even if it is smaller [55,56]. This fact is particularly important, especially when taking into account that the dominant donor species for the outer *n*-type oxides is oxygen vacancy [55,57]. The reduction in the charge carrier density in the passive film decreases the conductivity of the film itself, and thus a better stability may be hypothesized [55,58].

2.3. Effect of N and C on Corrosion Behavior

2.3.1. Nitrogen

N is added as an alloy element in austenitic stainless steels [3,59]. It has been proposed that a N-alloyed austenitic stainless steel be considered "high N" when N content is higher than 0.4 wt.% [59,60]. In austenitic stainless steels, N is used as a small addition in traditional steels, as occurs in AISI 316LN (~0.1–0.16 wt.%), and in larger amounts in high-N austenitic stainless steels and Ni-free austenitic stainless steels (0.45–1.1 wt.%), in which it is the substitute of Ni together with Mn [60,61].

Besides its ability to improve tensile properties [59,60,62], N also has a remarkable effect on corrosion behavior [4,59,60,62]. A beneficial effect is recognized when localized corrosion phenomena occur [4,59,60]. N is able to promote passivity, widen the passive range, and enhance the resistance to stress corrosion cracking and to intergranular corrosion [4,60,63–65]. The protection mechanism is still not completely clear, and different theories have been proposed. The primary suggestions are the following.

1. When interstitial N atoms are released during the early stages of the corrosion process, they may react with H^+ and form ammonium (NH_4^+) ions, following the subsequent reaction [65]:

$$N + 4H^+ + 3e^- \rightarrow NH_4^+ \quad (1)$$

   The formation of ammonium ions consumes protons, and then it locally increases the pH value in incipient pits or crevices and promotes repassivation [63,65–69]. At fairly high potential, nitrates (NO_3^-) are reported to form [63,69] (Figure 3), and is hypothesized that they are adsorbed at the surface of the passive film and may act as inhibitors [70]. Moreover, it is suggested that ammonium ions may form nitrates [66,69], that they may react with free chlorine in chlorinated water and form species which are less effective oxidants [71], or they may produce a passive ammonium sulfate layer in sulfate solutions [72].
2. Negatively charged N ($N^{\delta-}$) may accumulate at the passive layer and may have a repulsive action towards Cl^-, promoting a faster repassivation [68,73]. It is also suggested that $N^{\delta-}$ may change into ammonium ions [73].
3. During passivation, an enrichment of N occurs at the passive film/substrate interface, preventing anion attack [53,67]. An incorporation of N and ammonium ions in the passive film is also observed [53].
4. First-principles calculations suggest that interstitial N causes a decrease in the electronic density of states (DOS) of Fe at and near the Fermi level, and thus that it has a stabilization effect on the electronic structure and tends to suppress electrochemical reactivity [69].

When N-rich expanded austenite forms, the local alkalization of the solution according to (1) is the main mechanism invoked to justify the increase in localized corrosion resistance [22,74,75]. The formation of NH_3 and NH_4^+ species is observed on the outermost surface of the passive layer formed on N-rich expanded austenite subjected to anodic polarization in a 3 wt.% NaCl solution [49]. Using XPS analysis, Lei and Zhu [49] detect N, which was bonded with Cr and Fe, in the passive film and hypothesize that, during the early stages of anodic polarization, N is released onto the passivating surface while stable oxides form, and thus it is able to form NH_3. It is supposed that, as N is released, two-step N hydrolysis to NH_4^+ may occur. In the first step, N hydrolyzes to NH_3 with a very fast reaction rate, which is affected by the concentration of released N and not by the

pH value of the solution, and in the second step NH_3 further hydrolyzes to NH_4^+ with a slow reaction rate, one which becomes faster as the pH of the solution lowers [76].

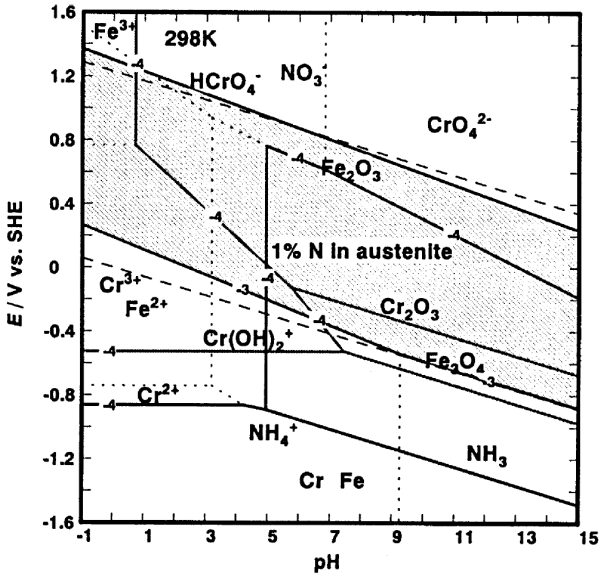

Figure 3. E–pH diagram for interstitial N, Fe and Cr. (For further details, see Ref. [63]) (Reprinted with permission from Ref. [63]. Copyright 2002 Elsevier).

Flis-Kabulska et al. [75] observe a local increase in pH due to N using in situ measurements for plasma-nitrided AISI 316L tested in deaerated solutions of 0.1 M Na_2SO_4 + 0.4 M NaCl acidified down to pH 2.4. The authors register an increase in pH at the surface of the nitrided samples and ascribe this alkalization to the formation of ammonium ions. It is hypothesized that the increase in corrosion resistance is related to a more efficient repassivation of incipient pits, which is occurring due in turn to the formation of oxides, promoted by the local alkalization, and to the formation of inhibiting NO_2^- anions, rather than due to a slow pit nucleation process.

It is also hypothesized that the strong bond between Cr and N may play a role in this process. In fact, as recalled before, in the passive film Cr and N enrichment is observed in the inner region, and thus the strong Cr-N interaction has the potential to restrict Cr migration [51].

A further effect may be due to the change in the semiconducting properties of the passive film formed on N-rich expanded austenite. The lower donor density in the outer *n*-type region of the passive layer, consisting mainly of Fe oxide/hydroxide, may decrease the pitting nucleation ability, hindering the Cl^- adsorption [54], and it allows to obtain more protective film [55,57].

Taking into account all the experimental results, it may be hypothesized that both the local alkalization of the solution and the changes in the characteristics of the passive film have roles in mitigating the corrosion phenomena.

When general corrosion is taken into account, both positive [59,77,78] and negative [60,79] effects of N alloying are reported.

2.3.2. Carbon

C improves the mechanical properties of stainless steels. However, from a corrosion resistance point of view, its use is considered detrimental [3,4]. Low C content is used in order to stabilize the passive layer and reduce the risk of sensitization [3,4].

The formation of C-rich expanded austenite highlights that C is able to improve resistance to localized corrosion, in particular increasing the corrosion and pitting potential. Different mechanisms are hypothesized as explaining this beneficial effect. A first hypothesis by Martin et al. [80] suppose that C atoms present in the passive film act as mobile

interstitials and enhance/maintain the oxygen vacancy motion. Heuer et al. [52] suggest that the improvement in corrosion resistance is related to the lower thickness of the passive film at a given potential, thus reducing the detrimental effect of the thickness undulation of the oxide film, which can cause dielectric breakdown and pitting nucleation. A recent hypothesis suggests that the carburized layer decreases the mobility of charge carriers in the passive film, since a decrease of the oxygen vacancy concentration occurs as the C content is higher, which is due to the strong Cr-C bonds forming at the metal-passive film interface [81]. This hypothesis is in accordance with the lower donor density observable in carburized specimens, which in turn is related to a decrease in the density of oxygen vacancy in the passive film and thus to a more stable and protective film [55,56]. Li et al. [82] suggest that C may weaken the passive film, but that, owing to the formation of localized covalent bonds with the metal atoms, it tends to immobilize metal atoms and thus metal dissolution becomes more difficult.

3. Austenitic Stainless Steels

The formation of an expanded phase was firstly recognized in austenitic stainless steels, as outlined by Borgioli [24] for low-temperature nitriding and by Christiansen and Somers [29] for carburizing treatments. Today, the most widely used names for the expanded phase formed in this stainless steel type are "expanded austenite", "S-phase" (with reference to the shift in its diffraction peaks in comparison with those of the untreated austenite), γ_N for the N-rich phase and γ_C for the C-rich phase (for all the used names, see [24] and the reference therein). The main characteristics of N- and C-rich expanded austenite, formed by means of nitriding or carburizing, are reported in Table 1.

Table 1. Main characteristics of the modified surface layers containing expanded austenite, obtained by nitriding or carburizing austenitic stainless steels.

Properties	Nitriding	Carburizing
Formation temperature (without formation of Cr compounds) (°C)	300–450	300–550
Max. interstitial content in expanded austenite (at.%)	38	19
Max. surface hardness	1450	1000
Hardness profile	abrupt change	gradual change

3.1. Microstructure and Characteristics of the Modified Surface Layers

The "colossal" supersaturation of interstitial atoms in the austenite lattice has an initial important effect in that it produces localized plastic deformations, which are observable starting from the surface. Slip bands are present inside the grains, crossing them in different directions depending on crystallographic orientations. Subsequently, a swelling and a rotation of the grains occur, causing the presence of reliefs at grain boundaries and the leaning forward of some grain boundaries onto adjacent grains [83–87] (Figure 4a). This peculiar surface morphology was observed in samples treated with both plasma- [83–86,88] and gas- [89,90] based processes, and on nitrided [83–86,88,89], carburized [91–93] and nitrocarburized [94] samples. As a consequence, even when starting from polished untreated samples, a surface roughness increase is obtained after the treatment [85].

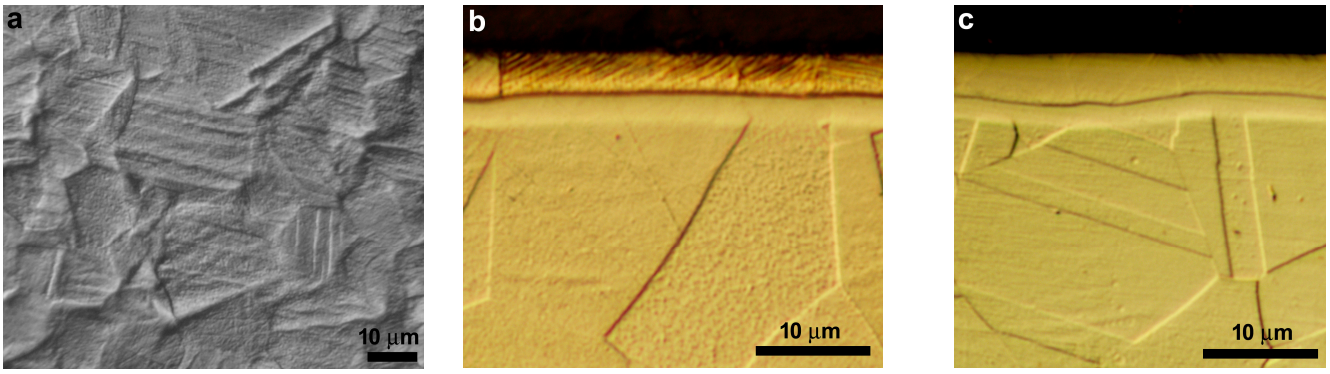

Figure 4. Surface morphology (**a**) and cross-sectional micrographs of a nitrided AISI 202 (**b**) and of nitrided AISI 316L (**c**) austenitic stainless steels (etchant: acetic glyceregia). (Nitriding conditions: 380 °C, 340 Pa, 5 h) (For further experimental details, see Ref. [95]).

Further interesting features can be observed at the cross sections and tapered sections of the treated samples. The high corrosion resistance of the modified surface layer consisting of expanded austenite can also be inferred by the fact that some of the chemical etchants usually employed for delineating the microstructure of stainless steels, such as Marble's reagent are not able to etch onto it [96,97]. The presence of a continuous and fairly homogeneous but almost featureless layer, separated from the matrix by a strong etched line, suggested that the "new" phase could be a nitride [24]. However, when using etchants such as glyceregia, additional features can be observed. When nitriding [95,98–103] and nitrocarburizing [28,94,104] are performed, the modified layer consists of a two-layer microstructure; conversely, in carburized samples, only one layer is present [28,55,105–107]. It was hypothesized that the strong etched lines, which separated the two modified layers and the substrate, were due to the sudden change in N concentration and as a response to chemical etching, and that they were not thermodynamic or crystallographic interfaces [102]. Grain boundaries were observable in the modified layer, and they were the continuation of those found in the austenite matrix [83]. In the two-layer microstructure, thin lines were observed in the outer layer, and it was suggested that they were slip lines occurring as the consequence of local plastic deformations induced by the solubilization of a large amount of N [108]. The number and the extension in the substrate of these slip lines depend on the nitriding conditions and steel composition [95,99,108]. As an example, in Figure 4b, the cross-sectional microstructure of the low-Ni CrMn AISI 202 steel, nitrided at 380 °C for 3 h, is depicted; as a comparison, the microstructure of the CrNi-grade AISI 316L, nitrided in the same conditions, is shown in Figure 4c.

The main constituent of the modified layer is expanded austenite, which is usually regarded as a supersaturated solid solution of interstitial atoms in the f.c.c. austenite lattice. The X-ray diffraction patterns of this phase have a peculiar feature since the peaks are shifted towards lower angles in comparison with those of austenite, with an apparently anisotropic expansion [24,28,33,84,109] (Figure 5). The nature of this expanded phase is still an open question. Many studies carried out with different analytical techniques suggested that a preferential bonding of N with Cr atoms occurred [110–112] and that Cr-N short-range order (SRO) regions were present together with regions having a γ'-Fe_4N-like long-range order (LRO) region, indicated as $\gamma_N{}'$ [113–116]. Further details on the structure of the expanded austenite are reported in [22,24,33].

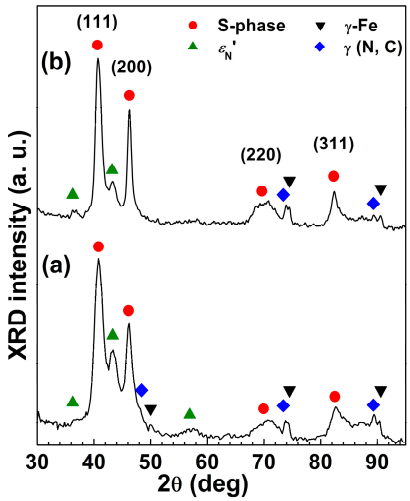

Figure 5. X-ray diffraction patterns of nitrided AISI 202 (**a**) and AISI 316L (**b**) austenitic stainless steels (Nitriding conditions: 380 °C, 340 Pa, 5 h) (For further experimental details, see Ref. [95]).

Together with expanded austenite, another N-rich phase is detected in the outer modified layer of nitrided samples, the so-called N-induced h.c.p. martensite, ε_N', which is a solid solution of N in the h.c.p. martensite, ε' [117]. The formation of this phase was hypothesized to be related to the local plastic deformations. Tao et al. [118] suggested that ε_N' formed from expanded austenite through a martensitic shear transformation which occurred above a critical N concentration. On the contrary, Tong et al. [119] ascribed these h.c.p. regions to "clustered" stacking faults instead of plates of N-rich h.c.p. ε' martensite. The formation of ε_N' depends on both solubilized N content and steel composition, and is promoted in steels with a low stacking fault energy, as well as in those with a high Mn content [88,95,99]. As an example, in Figure 5 the X-ray diffraction patterns of high-Mn low-Ni AISI 202 and low-Mn CrNi AISI 316L austenitic stainless steels, which were nitrided at 380 °C for 3 h, are depicted. The ε_N' phase can also be the precursor to h.c.p. ε-$Fe_{2\text{-}3}N$ nitride, which may have formed from it as a result of the ordered arrangement of N atoms and the distortion of the lattice [120].

The formation of ε_N' and the γ_N' LRO phases, which can be regarded as the precursors of ε and γ' Fe-nitrides, is not peculiar to nitrided samples, as these phases were also detected on nitrocarburized specimens [121].

The presence of an inner modified layer is assessed well when the nitrocarburizing treatment is performed, and it is ascribed to the formation of a C-rich expanded austenite [28,94,104,122]. When nitrided samples were analyzed, an inner layer was not detected by all the authors. Borgioli et al. [108] observed an inner modified layer on AISI 202 samples which had been glow-discharge-nitrided at 380 °C. By performing X-ray diffraction analysis at different incident angles, the authors assessed that this layer could be related to the presence of a f.c.c. phase as it had a lattice parameter slightly larger than that of austenite. The formation of this phase, which can be regarded as a solid solution of interstitial atoms (N, C) in austenite, γ(N, C), was observed both in steels having both a fairly high C content, such as 202 and Ni-free steel, and a low C content, such as AISI 316L [95,108,123–125], so that the hypothesis that this is only related to a local increase in C atoms [126], pushed ahead by diffusing N atoms, is not completely convincing. Williamson et al. [98] suggested that it may be due to the high residual stress, induced between the expanded austenite layer and the substrate, while Christiansen et al. [102] hypothesized that it may be related to the N concentration profile. Recently, in 316Ti steel subjected to N low-energy ion implantation in order to study the initial phase of nitriding, Manova and Mändl [127] observed the formation of a low-expansion f.c.c. phase, that subsequently transformed into expanded austenite when the N content increased.

Nitrides are usually observable in the outer modified layer as strong etched zones; these are present especially along the slip lines and grain boundaries. When CrN is able to form, the loss of solubilized Cr from the matrix has the potential to cause a transformation of f.c.c. austenite into b.c.c. α-Fe [128]. The maximum temperature at which Cr-compounds do not form is usually 450 °C for nitriding [27,60] and 550 °C for carburizing [27]. However, the temperature, at which nitride precipitation occurs, depends on steel composition, and tends to decrease as the Mn-content increases and Ni-content decreases [99,123,129,130]. Moreover, the nitride precipitation also depends on the treatment duration and N feeding [84,123,125,129,131]. Similarly, C solubilization and carbide formation also depend on alloy composition [93,107].

The concentration profile of interstitial atoms in the modified layers depends on the treatment used. In nitrided samples, N concentration has high values at the surface, a steep decrease to lower values, followed by a nearly constant plateau, and then a steep decrease to matrix values [22,24,28,102]. In carburized samples, C concentration decreases steeply near the surface and then more smoothly to the matrix values [22,24,28,55]. In nitrocarburized samples, the formation of an outer layer consisting of N-rich expanded austenite and an inner layer, in which C-rich expanded austenite is present, produces a smoother profile, as compared to those of nitrided steels [24,28,132]. The maximum N content solubilized in expanded austenite is 38 at.% [42], while the maximum C content is 19 at.% [43].

The huge interstitial atom solubilization causes an increase in surface hardness. A maximum surface hardness of ~1450 kg_f mm^{-2} is registered for nitrided steels [131], and a maximum surface hardness of ~1000 kg_f mm^{-2} is observed for carburized ones [133]. The microhardness profiles resemble those of interstitial atom concentration. For the nitrided samples, the microhardness profiles usually show an abrupt decrease from the high hardness values near the surface to the matrix values. Conversely, for the carburized specimens, a more gradual decrease in hardness values is registered [24,104]. Nitrocarburizing allows to obtain high microhardness values at the surface together with a smoother hardness profile [24,104].

Further details on the characteristics of the modified layers are summarized in [22,24,26,33].

3.2. Corrosion Behavior in Presence of Cl^-

The presence of Cl^- ions in an aqueous environment may be harmful for austenitic stainless steels. since these ions are able to weaken the protective effect of the passive film and cause localized corrosion phenomena, such as pitting and crevice, and promote stress corrosion cracking when a tensile stress is applied. General corrosion may occur in HCl solutions. The corrosion resistance characteristics of the modified surface layers, obtained on austenitic stainless steels by means of nitriding or carburizing, are summarized in Table 2.

Table 2. Corrosion resistance in Cl^--containing solutions of the modified surface layers obtained on austenitic stainless steels by means of nitriding or carburizing.

Solution	Modified Layer Type	Nitriding	Carburizing
NaCl	- expanded austenite only	very good	good
	- with martensite	very good–good	-
	- with nitrides (low amount)	acceptable	-
Body fluid-like	- expanded austenite only	good	good
	- with martensite	good	-
$NaCl + Na_2SO_4$	- with martensite/nitrides [1]	good	-
$FeCl_3$	- expanded austenite	good	good
HCl	- expanded austenite	good	good

[1] Hypothesized on the basis of nitriding conditions and X-ray diffraction pattern.

3.2.1. Electrochemical Impedance Spectroscopy (EIS) Analysis

EIS analysis is a powerful tool for investigating the general corrosion resistance of modified surface layers. For stainless steels, the Nyquist plot is characterized by the presence of a single semicircle [134,135] or two connected semicircles [135–138], which are characteristic of one time constant or two time constants, depending on the test conditions. By modeling the experimental data with an electrical equivalent circuit (EEC), it is possible to obtain a physical picture of the corrosion phenomena. The semicircle trend can be modeled using a Randles circuit, i.e., a solution resistance element in series with the parallel combination of a resistance element, R, and capacitance, C. These are identified with the charge transfer resistance and double-layer capacitance [139]. When two connected semicircles are observed, the data can be modeled with two parallel combinations of R and C, either hierarchically connected [78,135,140–142] or in series [143]. When a model with two time constants is required, one constant is usually connected to the charging/discharging processes that take place at the interface between the electrode and the electrolyte, whereas the other is connected to the charge transfer and mass transport processes that occur in the oxide phase. However, their attribution to the low or high time constant is not univocal [78,135,138,141]. The sum of the resistance elements (charge transfer resistance and oxide-related resistance) is usually indicated as polarization resistance and it can be considered a measure of the surface total resistance to general corrosion [138].

When low-temperature nitriding produced modified surface layers consisting essentially of expanded austenite, for tests in NaCl solutions, in the Nyquist plot the semicircle of nitrided samples was usually wider than that observed for untreated alloys, suggesting a better corrosion resistance [54,95,124,144]. When the experimental data were depicted in a Bode plot, higher impedance values were reported and, in the analysis of a phase angle plot, the presence of a second inflection at a lower frequency was registered, meaning that two time constants could be hypothesized [54,95,123,124,145]. As examples, the Nyquist and Bode plots of untreated and nitrided AISI 202 samples are shown in Figure 6.

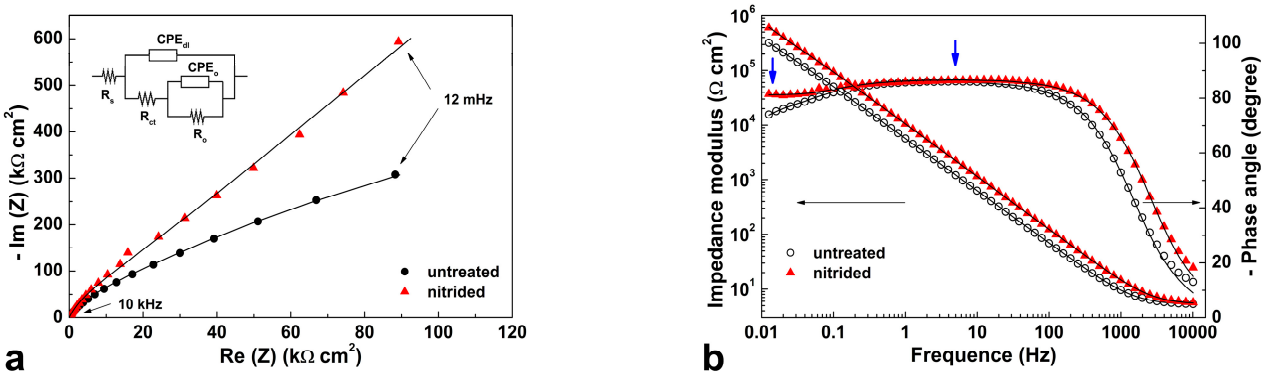

Figure 6. Nyquist plots (**a**) and Bode plots (**b**) of untreated and nitrided (380 °C, 340 Pa, 3 h) AISI 202 samples, recorded at the respective open circuit potentials (symbols: experimental data; lines: modeled data using the equivalent electrical circuit drawn in (**a**)). For the circuit: R_s, electrolyte resistance; R_{ct}, charge transfer resistance, CPE_{dl}, double layer/space charge capacitance, R_o, resistance of the oxide layer, and CPE_o capacitance/mass transfer processes in the oxide layer) (solution: 5 wt.% NaCl, aerated). (The blue arrows in the phase angle plots indicate the two inflections of the plot.) (For further details, see Ref. [95]).

As was observed for the untreated alloys, the attribution of the different processes to the two time constant elements is not univocal. Borgioli et al. [95,123], who tested untreated and nitrided austenitic stainless steel samples in 5 wt.% NaCl solution, fitted the EIS data using two parallel R–C elements, hierarchically connected, and they related the high-frequency (HF) time constant to the faster charging/discharging processes occurring at the electrode/electrolyte interface, while the low-frequency (LF) time constant was linked to the slower processes taking place in the oxide phase. Pure capacitance elements

were substituted with constant phase elements (CPE). It was observed that, for the HF time constant, the CPE exponent, n, was usually very close to unity [95,145], so that it was hypothesized that the behavior of the double layer deviated from that of a pure capacitance structure (n = 1) due to surface heterogeneities at the atomic (surface disorder as dislocations and steps, chemical inhomogeneities) and micrometric (roughness, polycrystalline structure) scales and due to adsorption phenomena [136,141]. For the LF time constant, a tendency to a significant decrease in CPE exponent was observed in comparison with that of untreated steels [95]. It was usually suggested that this fact may be due to surface heterogeneities [136,141], diffusion phenomena in the oxide film [136], and variation in oxide composition, each of which caused a distribution of resistivity and dielectric constant [146]. A reduction in the capacitive contribution of the oxide film was observed in the nitrided samples [95], as was a marked increase in the resistance of the oxide film, which enhanced corrosion resistance [95,145]. A similar interpretation of the two time constants was given by Zhu et al. [54], who modeled the EIS spectra using a solution resistance element in series with two parallel combinations of R and CPE and ascribed the HF time constant to the charge transfer process at the expanded austenite layer/electrolyte interface and the LF time constant to the occurrence of the diffusion process through the passive film. It has to be noted that for the nitrided steel, with this attribution to the two time constants, the resistance ascribed to the oxide film was higher than that related to the charge transfer resistance at the electrode/electrolyte interface [54,95,123]. However, the overall polarization resistance increased for the nitrided samples, in comparison with the untreated steels [54,95,123].

The formation of low amounts of N-rich h.c.p. martensite, ε_N', together with expanded austenite does not significantly affect the corrosion behavior of nitrided samples. Studies carried out on different austenitic stainless steels (AISI 316L, AISI 202 and Ni-free P558), nitrided at 360 and 380 °C, showed that similar trends of impedance data were observed when samples were tested in 5 wt.% NaCl aerated solution [95]. However, when the ε_N' amount was fairly high and the h.c.p.-based ε-nitride could form, as for P558 Ni-free austenitic stainless steel samples nitrided at 380 °C, three inflections were observed in the phase angle plots, suggesting the presence of three constant phase elements [95,123]. Models with three hierarchically connected time constants were used for inhomogeneous surfaces [147] or porous oxide films [148]. As a result, it was hypothesized that the (1) element was related with a heterogeneous and/or porous oxide layer, that the element (2) with the processes taking place at the electrode/electrolyte interface, and that the (3) element with the processes occurring in the inner compact oxide layer. Nevertheless, a fairly high polarization resistance was observed for these samples.

Luiz et al. [149] studied the change in EIS spectra over a timeframe ranging from 1 h to 30 days for a nitrided UNS S31254 super-austenitic stainless steel, which the authors tested in a 3.5 wt.% NaCl aerated solution. In the Nyquist plot, the semicircles became wider as the test duration reached 7 days. Then, after 15 and 30 days, a slight decrease was observed. The authors used an EEC with two parallel R–C elements hierarchically connected, but related the HF time constant to the passive film formation, the LF time constant to the charge and the mass transfer phenomena, occurring through the passive film, to the double layer. With this model, the higher resistance values were related to the charge transfer resistance, while the passive film resistance had lower values. The polarization resistance was at a maximum for 7 days; then, it slightly decreased, and it was comparable to that of the untreated steel. The estimated passive film capacitance was slightly lower than that of the untreated alloy and did not change significantly, suggesting the formation of a highly stable film which did not undergo relevant dissolution processes.

When significant amounts of nitrides formed, narrower semicircles in Nyquist plots are observed, meaning that a decrease in corrosion resistance may be supposed [123].

Nitrocarburized samples have a behavior similar to that observed for nitrided ones, with wider semicircles in the Nyquist plots and higher impedance values in the Bode plots when mainly expanded austenite is able to form [94].

A higher corrosion resistance is also hypothesized for C-rich expanded austenite, since wider semicircles in the Nyquist plots [56,81] and higher impedance values in the Bode plots [55,56] are observed.

3.2.2. Open Circuit Potential Measurements

Even if there was usually a delay before electrochemical tests were performed to allowing the sample to reach an equilibrium condition in the solution, data regarding open circuit potential (OCP) measurements, which allow researchers to evaluate the behavior in free corroding conditions, were seldom reported.

The OCP of the untreated alloys usually shows sharp decreases and increases due to metastable pit nucleation and repassivation phenomena [30,150]. As the delay duration increases, different trends are observable, showing either increases [131] or decreases [95] in OCP values, as depicted in Figure 7. The increasing trend is typical of passive materials, which may be related to the passivation effect in the solution on freshly polished samples [151]. However, for fairly long delay durations, a decrease is also observed, which may be ascribed to a degradation of the air-formed passive layer due to the absorption of Cl^- [8,130,152,153]. A subsequent potential increase such as that observed by Borgioli et al. [95] may be ascribed to repassivation phenomena.

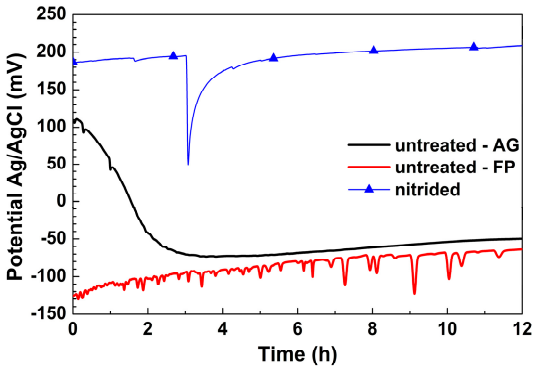

Figure 7. Open circuit potential vs. time for AISI 316L samples: untreated with air-grown passive film (AG) and freshly polished (FP); nitrided at 380 °C for 3 h (air-grown passive film) (for further details on the treatment, see Ref. [95]) (solution: 5 wt.% NaCl, aerated).

When expanded austenite is able to form, an increasing trend of OCP values is registered in NaCl aerated solutions, and the potential values are higher than those of the untreated alloys [95,131,150] (Figure 7). Fluctuations are also observed due to metastable pit formation and repassivation. However, the pit nucleation events are fewer than those of the untreated alloy [131,150], and the pit repassivation kinetic tends to be slower than that of the alloy [95,131,150]. The formation of a considerable amount of nitrides causes a decrease in OCP values, probably due to the occurrence of many corrosion events on the surface [150].

The study of the OCP values up to 30 days for the nitrided UNS S31254 superaustenitic stainless steel tested in a 3.5 wt.% NaCl solution showed that, after a fast increase during the first day, OCP tended to increase more slowly and had a maximum value at 15 days of immersion in the probe solution and then experienced a slight decrease [149]. It was hypothesized that a slow dissolution process of the passive film took place for immersion periods longer than 15 days.

The experimental data present in the literature suggest that equilibrium conditions may be attained by the treated alloys with fairly long durations. This fact should be taken into account when the delay time is chosen before electrochemical tests.

3.2.3. Localized Corrosion Phenomena in NaCl Solutions

NaCl solutions are the most commonly used test solutions to assess the localized corrosion behavior of alloys, and electrochemical techniques are usually employed, such as potentiodynamic polarization, cyclic potentiodynamic polarization, potentiostatic and galvanostatic measurements, together with crevice tests. It has to be taken into account that the different experimental results presented in the literature depend on both the test conditions and the characteristics of the modified layers, and so a direct comparison cannot be straightforwardly performed.

When low-temperature nitriding treatments are carried out and modified surface layers formed, consisting of N-rich expanded austenite, the polarization curves possess the typical features showed by N-containing austenitic stainless steels, as depicted in Figure 8a. When compared to the untreated alloy, the nitrided samples usually have higher corrosion potential, lower anodic current density in the passive branch and higher pitting potential [22,30,54,74,95,129,149,154,155]. As a consequence, after the tests it was found that the surface of the nitrided samples showed fewer pits than the untreated steel, or seemed fairly untouched, with micrometric or submicrometric pits that could be observed only using microscopic techniques [95,108,150] (Figure 8b,c). A slight change in color was sometimes observed, which could be ascribed to the transpassive dissolution of the oxide film, due to the high potential values reached in the test [95]. It has to be recalled that the localized corrosion phenomena produced by potentiodynamic polarization tests may cause both pits and crevices, which may occur in the area shielded by the gasket.

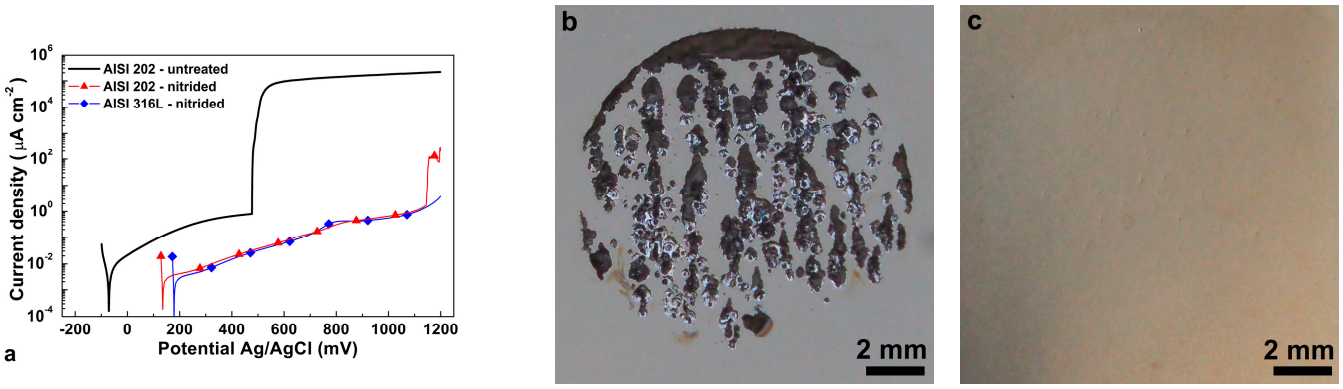

Figure 8. Corrosion behavior of AISI 202 (untreated and nitrided) and AISI 316L (nitrided) (nitriding conditions: 380 °C, 340 Pa, 3 h): polarization curve (**a**), details of the surface morphology after corrosion test of untreated (**b**) and nitrided (**c**) AISI 202 samples (solution: 5 wt.% NaCl, aerated). (For further experimental details, see Ref. [95]).

The protection effect of expanded austenite and its ability in hindering and delaying the occurrence of corrosion phenomena tend to increase as the N content in this phase is higher, the precipitation of significant number of nitrides is avoided, and the modified surface layer is thicker. Thus, treatment temperature, duration and N feeding have to be chosen in order to produce a N-rich, nitride-free and thick modified layers [83,84,95,123,124,129,131,150,156]. It has to be noted that the localized plastic deformations, which cause the increase in surface roughness and the formation of N-induced h.c.p. martensite, ε_N', do not significantly impair the protectiveness of the modified layer. The presence of deformation bands in N-alloyed austenitic stainless steel, present due to cold working conditions, was reported to increase the number of sites for pitting nucleation and reduce corrosion resistance [157]. On the contrary, even in nitrided austenitic stainless steels showing a large amount of localized plastic deformations in the modified surface layers, such as AISI 202, an improvement in corrosion resistance was registered due to expanded austenite [99,108,129]. A similar observation was made by Lei et al. [158], who obtained comparable (high) corrosion resistance in a 1 wt.% NaCl solution for modified layers of

nitrided 1Cr18Ni9Ti steel which consisted of expanded austenite with and without ε_N'. Similarly, Tao et al. [130] observed that the formation of N-induced expanded martensite did not have a detrimental influence on the corrosion resistance of the nitrided (400 °C, 20 h) high-Mn Staballoy® AG 17 steel tested in 3.5 wt.% NaCl solution.

A peculiar behavior was registered by Borgioli et al. [95,123] on nitrided Ni-free austenitic stainless steels, either as the treatment temperature increased (380 °C) or at lower temperatures (360 °C) for longer durations (5 h). With these treatment conditions, the modified surface layers had a high density of slip lines, even if no detectable amount of nitride precipitates was observed. These samples had a higher corrosion potential when compared to that of the untreated alloy, as well as lower anodic current density values in the passive branch up to approximately +630 mV (Ag/AgCl). For higher potential values, an increase in anodic current density was registered, up to a maximum at about +960 mV (Ag/AgCl), and then a decrease occurred down to values of a second passive branch, suggesting the occurrence of oxidation phenomena. It was hypothesized that oxidation phenomena might be promoted by the heterogeneous structure formed by expanded austenite with a fairly large amount of h.c.p. phase (ε_N' and/or submicrometric nitride precipitates), which might hinder repassivation. However, a very small anodic current density peak was observed at about the same potential values for other nitrided austenitic stainless steel types, such as AISI 316L [95,129], AISI 304L [99] and AISI 202 [99,129]. On the basis of the Pourbaix diagrams of the main alloy elements [63,159] and taking into account an acidic solution, as the one expected for pitting or crevice phenomena, it was hypothesized that this anodic current peak was related to the oxidation of Cr(III), mainly in form of Cr_2O_3, into Cr(VI).

The effect of inclusions, such as MnS, on the corrosion resistance of the modified surface layers, consisting of N-rich expanded austenite, was recently studied [160]. The inclusions appeared to be pitting initiation sites, but they did not cause pitting or crevice in the expanded austenite. In fact, localized corrosion occurred in the untreated substrate, beneath the modified layer, where the electrolyte was able to penetrate due to the partial dissolution of the inclusions. Thus, as observed before, the protective effect of the expanded austenite was higher when thicker modified layers formed.

The effect of alloy elements on the corrosion behavior of nitrided austenitic stainless steels was also studied [95,99,129,161]. The comparison of the potentiodynamic curves of AISI 316L, AISI 202 and Ni-free P558 steel samples, nitrided at 360 and 380 °C and tested in a 5 wt.% NaCl aerated solution, suggested that the corrosion potential and anodic current density values were influenced mainly by the solubilized N, and that the pitting potential depended on both the N content and alloy elements [95]. In particular, Mo-containing alloys had an improved corrosion resistance after nitriding due to the synergy of Mo and N in hindering corrosion phenomena [95,99,161].

The influence of surface finishing on the corrosion behavior was also assessed [124]. It is well known that a smoother surface has a higher corrosion resistance since the possible sites for pits are more open, preventing the accumulation of Cl^- and H^+, so that metastable pits are less capable of propagating and a higher potential is required to cause a stable pitting [162]. However, surface roughness comparable to that obtained with a 2D finishing (Ra~0.2 μm) maintained a very good corrosion resistance when the samples were subjected to low temperature nitriding [124]. However, it has to be recalled that localized plastic deformations occur when expanded austenite forms, and thus even a very smooth surface of an untreated steel increases its roughness after nitriding, but that the rougher surface does not impair the improvement in corrosion resistance due to N solubilization [95,124].

Nitriding treatment is also able to improve corrosion resistance in combination with a surface mechanical attrition treatment (SMAT). Li and Wang [163] carried out a duplex treatment consisting of a first SMAT step, which produced a nanostructured layer, and then a nitriding treatment (400 °C, 6 h). The duplex treated samples showed an improved corrosion resistance in comparison with the samples subjected to SMAT only.

The ability of the expanded austenite modified surface layers to repassivate is usually investigated using the cyclic potentiodynamic method. Different results were obtained with this technique. The repassivating potential was higher than that of the untreated steel [149], or it was lower [158,164], suggesting that repassivation did not occur, or was not measured [74,158], due to the transpassive dissolution of the passive film. These results may be ascribed to the different extent of the damage to the modified layer caused by this technique, which may hinder repassivation. The galvanostatic technique may be another useful technique for assessing repassivation, or protection, potential [165]. Galvanostatic tests highlight that, after the occurrence of localized corrosion phenomena, potential values below which corrosion did not occur were higher than those of corrosion potential, so that it was hypothesized that repassivation could occur when the depth of pits or crevices was not too large [95].

By using cyclic polarization tests, Zhu and Lei [74] obtained potential–pH diagrams for AISI 1Cr18Ni9Ti steel, untreated and nitrided at 380 °C for 4 h (N concentration in expanded austenite: 32 at.%), and tested in 3 wt.% NaCl solutions with pH values ranging from 0.4 to 13 (Figure 9). The formation of expanded austenite extended the immunity and perfect passivity zones and reduced the imperfect passivity and pitting regions in comparison with the untreated alloy. For pH 0.4–3, an active–passive behavior was observed for both untreated and nitrided specimens, with a change from general corrosion to imperfect passivity–perfect passivity–imperfect passivity–pitting corrosion, even if the pitting potential values of nitrided steel were higher than those of the untreated alloy. For pH 4–13, the untreated steel had the typical passive–transpassive transition due to pitting phenomena, while for nitrided samples the perfect passivity region was widened and pitting was not observed. Above pH 11, both sample types were resistant to pitting corrosion. On the basis of these results, it was hypothesized that the neutralizing effect of NH_4^+ ions in acidic pits was significantly only above a certain range of pH, and, in particular, that there was a significant improvement in pitting corrosion resistance in 3 wt.% NaCl solutions at pH values ranging from 4 to 11.

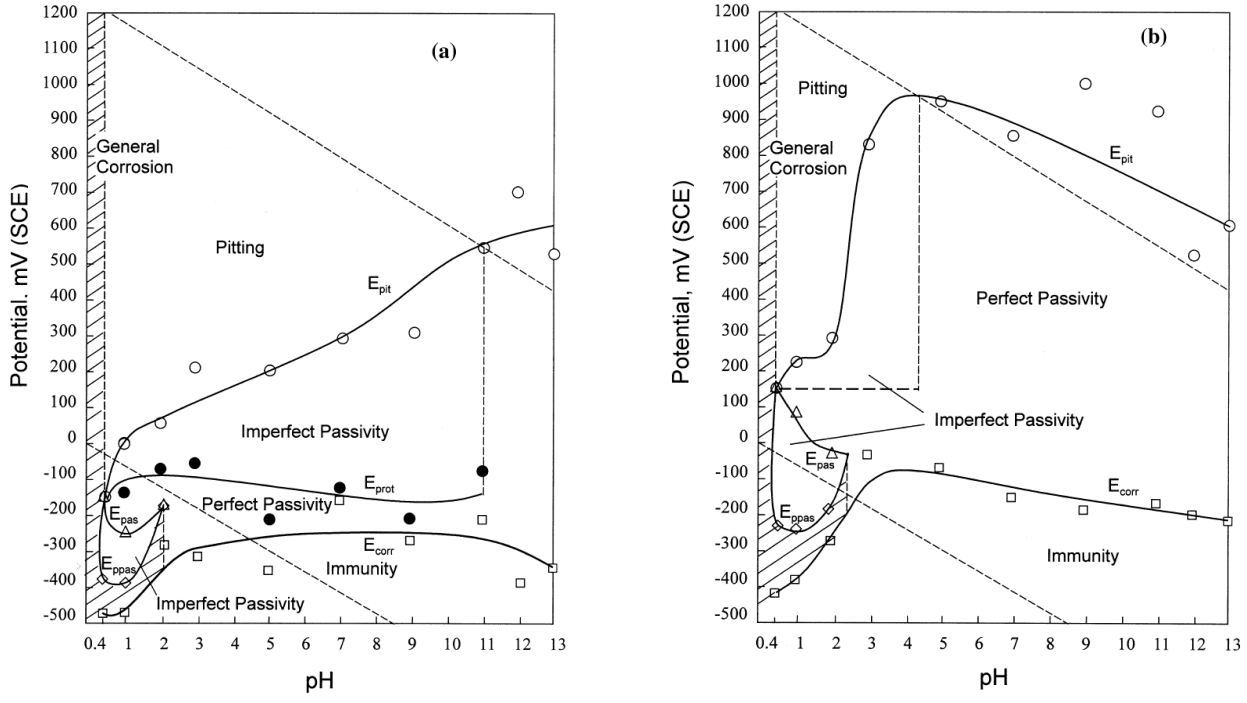

Figure 9. Potential–pH diagrams in 3 wt.% NaCl solutions for 1Cr18Ni9Ti: (**a**) untreated steel; (**b**) N-rich expanded austenite layer (For further details, see Ref. [74]). (Reprinted with permission from Ref. [74]. Copyright 2000 Elsevier).

The crevice tests highlight that low-temperature-nitrided austenitic stainless steels also have an excellent resistance to this type of localized corrosion. AISI 316L samples, plasma-nitrided at 430 and 400 °C for 5 h, did not have any observable crevice corrosion event after 60 days when tested in a 10 wt.% NaCl solution at 55 °C; meanwhile, for the untreated steel, the first corrosion attack occurred after only 3 days [150] (Figure 10). When the samples were nitrided at 500 °C, and a large amount of Cr nitride was able to form, the resistance to crevice corrosion markedly decreased.

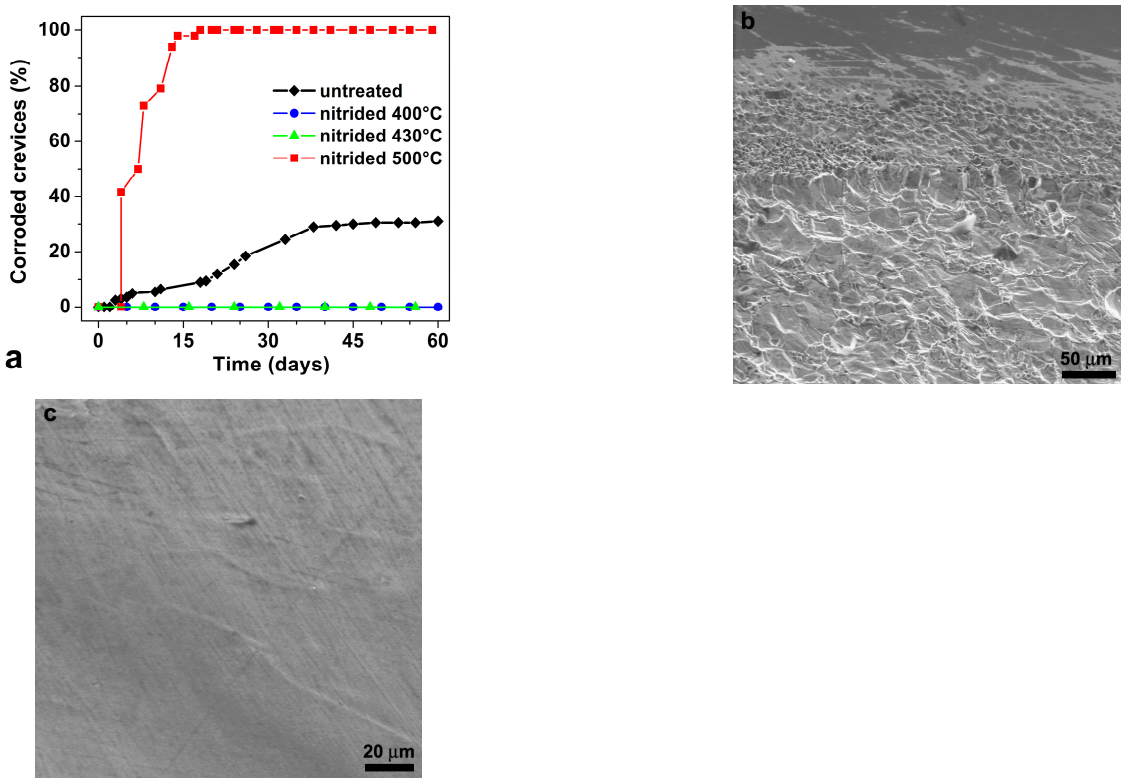

Figure 10. (**a**) Percentages of crevices, in which corrosion process are active, vs. time for AISI 316L samples untreated and nitrided as indicated (nitriding time: 5 h). Surfaces of AISI 316L samples untreated (**b**) and nitrided at 400 °C (**c**) after 60 days (solution: 10 wt.% NaCl, aerated, at 55 °C). (For further details, see Ref. [150]).

According to Olzon-Dionysio et al. [155], the improvement in corrosion resistance of nitrided samples might be due not only to N-rich expanded austenite, but also to the presence of ε and γ′ nitrides, which formed up to a depth of 0.1 µm and were detected by means of Mössbauer spectroscopy analysis. However, it is not clear whether these phases were really nitrides or they were the h.c.p. N-rich martensite, ε_N', and the LRO γ_N' phase, which were expected to form in the outermost layer where the N content was higher.

The formation of a small number of nitrides, together with expanded austenite, do not hinder the modified surface layers to exert their protective effect. Even if lower corrosion potential and slightly higher anodic current density values in the passive branch were observed, the pitting potential was usually higher and the damage on the surface was smaller than that of the untreated steel [84,96,99,108,124,150]. This significant improvement was not observed when crevice tests were performed [150]. When a large amount of Cr-rich nitrides forms, a marked decrease in corrosion resistance is registered [83,89,108,123,125,150].

For the nitrided AISI 316L steel, an increase in the critical pitting temperature from 40 to 65 °C was reported [166].

Nitrocarburizing is effective in improving corrosion resistance, increasing the corrosion potential and pitting potential values and decreasing the anodic current density in the

passive branch [94,104,122,167,168]. A slower pit formation was observed in the modified surface layer obtained on active-screen nitrocarburized AISI 316L, in comparison with that of both untreated and nitrided specimens, suggesting that C, in combination with N, acted in inhibiting the corrosion process [168]. The formation of N-rich Fe-based phases, ε_N' and the LRO γ_N', tended to cause an increase in the anodic current density in the passive branch, even if the passive branch was wider than that of the untreated steel [121].

Low-temperature carburizing causes an increase of corrosion resistance in NaCl solutions [25,55,56,106]. A significant increase in pitting potential, in comparison with that of the untreated alloy, is observed. A very good ability to repassivate is also registered when using cyclic potentiodynamic tests [25,55].

Sun [55] studied the corrosion behavior of carburized AISI 316L in a 0.5 M NaCl solution and pointed out that the high potential value (+1200 mV(SCE)) at which anodic current density increased was related to crevice corrosion phenomena, and not to stable pit formation. It has to be noted that this very good result was obtained by removing the first microns of the modified layer, in which a carbon soot and carbides might form. Moreover, by progressively removing the modified layer and repeating the cyclic potentiodynamic tests, similar polarization curves were registered both in the forward scan and in the reverse scan. In particular, it was observed that there existed a critical C concentration of ~0.25 wt.% (~1.1 at.%), above which C-rich expanded austenite had an excellent corrosion resistance without a significant dependence on the C content (Figure 11a). The very good corrosion resistance of the carburized layer was also assessed by performing potentiodynamic tests on the cross section (Figure 11b). The growth of pits near the modified layer was hindered; meanwhile, in the untreated substrate, pitting formed freely. Using potentiostatic tests, it was observed that metastable pit formation tended to be inhibited on carburized specimens. Very good corrosion resistance of the carburized steel was observed also in a 0.5 M NaCl + 0.5 M HCl solution.

For the carburized AISI 316, an increase in the critical pitting temperature was reported from 16.9 to 79.1 °C [25].

When treatment conditions allow the formation of carbides at the surface, a decrease in corrosion resistance is observed, with a smaller passive branch having higher anodic current density values [56].

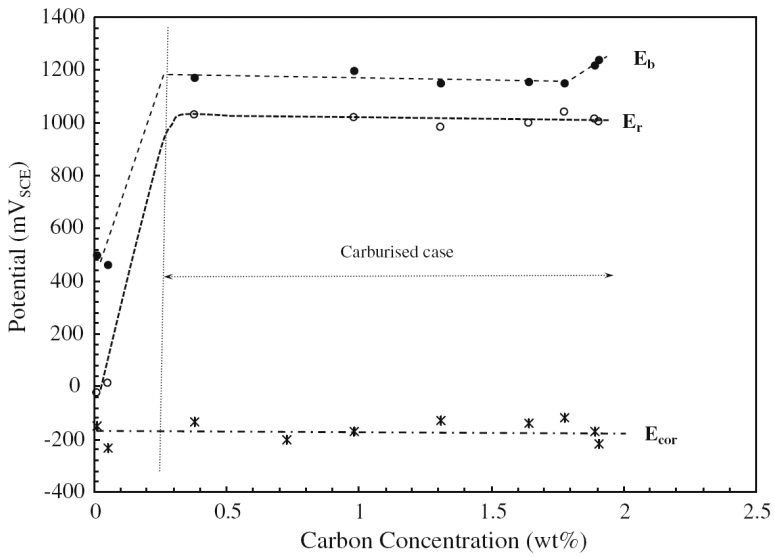

(**a**)

Figure 11. *Cont.*

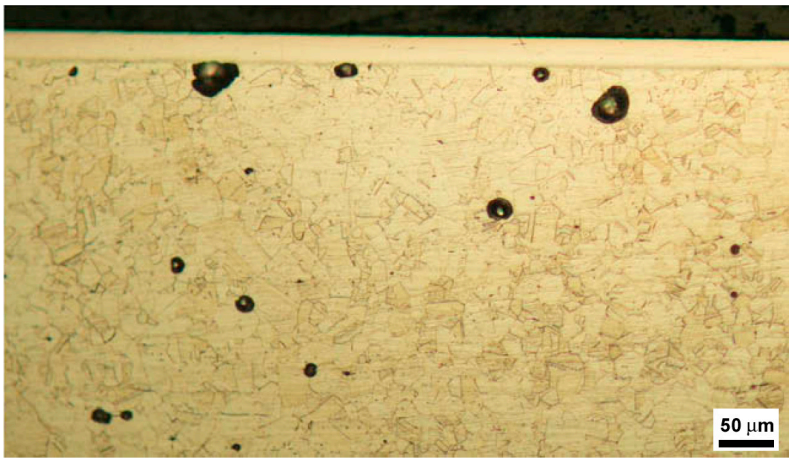

(**b**)

Figure 11. (**a**) Variation in corrosion potential (E_{cor}), breakdown potential (E_b) and repassivation potential (E_r) with C concentration for a carburized AISI 316L stainless steel. (**b**) Particular of the surface after potentiodynamic test on the cross section (chemical etching was performed after the test for delineating the microstructure) (solution: 0.5 M NaCl, aerated). (For further details, see Ref. [55]). (Reprinted with permission from Ref. [55]. Copyright 2010 Elsevier).

3.2.4. Localized Corrosion Phenomena in Mixed Saline Solutions

Electrochemical tests are also performed on low-temperature-treated austenitic stainless steels using solutions which contain NaCl together with other salts, such as those used for the simulation of body fluids.

An increase in corrosion resistance is observed for nitrided stainless steels tested in phosphate-buffered saline (PBS) solution [169–172]. The nitrided samples usually have higher corrosion potential and lower anodic current density values than the untreated ones [169,170,172]. Regarding the potential value at which the passive–transpassive transition occurs, higher values are not always registered for nitrided samples. For example, Martinesi et al. [170] observed comparable potential values for the passive–transpassive transition for AISI 316L samples, untreated or nitrided at 400 °C, 5 h, and tested in PBS, while similar samples registered a marked difference in pitting potential when tested in 5 wt.% NaCl [129] (Figure 12). It was hypothesized that the phosphates present in the PBS solution were adsorbed to the stainless steel surface and exerted their anodic inhibitor effect, thus delaying pit initiation [173].

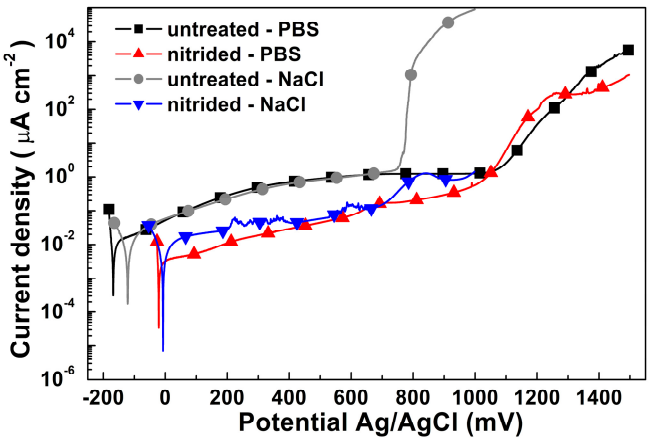

Figure 12. Potentiodynamic polarization curves of AISI 316L untreated and nitrided tested in PBS and 5 wt.% NaCl solutions (aerated). (For further details, see Ref. [170] (PBS) and Ref. [129] (NaCl solution)).

Lei and Zhu [174] tested untreated and nitrided (380 °C, 4 h) AISI 316L and 1Cr18Ni9Ti steels in Ringer's solution at pH values of 3.5–7.2 at 37 °C. When the solution was between pH 7.2 and 5.5, the nitrided samples did not suffered pitting corrosion due to the transpassive dissolution of the passive films on the surface. Conversely, for a pH of 3.5, a transition from passivation to pitting corrosion was observed, even if the pitting potential values of the nitrided steels were higher than those of the untreated alloys. The increase in corrosion resistance of plasma nitrided AISI 316L (350 and 400 °C, 2 h) was also observed when the samples were tested by means of potentiodynamic tests and EIS analysis in a simulated body fluid (SBF) solution [175].

The formation of a low amount of Fe-based nitrides did not impair the corrosion resistance of nitrided AISI 316L in Ringer's solution and a more extended passive branch was observed with lower anodic current density values in comparison with the untreated steel [96].

For the food and medical industries bacterial colonization is a major concern, together with corrosion resistance, and so antibacterial textures are employed. Dashtbozorg et al. [176] studied the effects of ultrashort pulsed laser texturing on the corrosion resistance of N-rich expanded austenite in Ringer's solution. The authors reported that the modified layers maintained a high corrosion resistance when femtoseconds laser pulses were employed. Conversely, when using laser pulses within the nanosecond regime the thermal decomposition of expanded austenite occurred and a worsening of corrosion resistance was observed.

When tests were carried out in a 0.4 M NaCl + 0.1 M Na_2SO_4 solution at pH 3, low-temperature-nitrided AISI 304L (425 °C, 30 h) had a higher resistance to pitting corrosion than the untreated alloy. N accelerated anodic oxidation in the initial stages of polarization, and promoted the subsequent passivation, mainly due to the precipitation of corrosion products [177]. It has to be pointed out that the used nitriding conditions might promote the formation of ε_N' martensite and nitrides precipitates, which might be responsible for the observed accelerated anodic oxidation in the initial stages.

An improvement in corrosion resistance is registered in Ringer's solution for nitrocarburized samples, whereby the treatment conditions inhibited the formation of precipitates [178], and also for carburized samples [178,179].

3.2.5. Localized Corrosion Phenomena in $FeCl_3$ Solutions

$FeCl_3$ solutions are often used for evaluating localized corrosion phenomena (see, for example, ASTM G48 standard—"Test Methods for Pitting and Crevice Corrosion Resistance of Stainless Steels and Related Alloys by Use of Ferric Chloride Solution").

Bottoli et al. [90] tested gas-nitrided AISI 316 (430 °C, 20 h) in a 3 wt.% $FeCl_3$ solution at pH 1 applying Teflon shaped washers in order to evaluate the resistance to crevice corrosion. After 168 h immersion duration (1 week) the weight loss of this sample type was significantly lower than that of the untreated alloy, confirming the very good resistance of low-temperature-nitrided austenitic stainless steels to crevice corrosion.

Crevice corrosion resistance on carburized 316LVM samples was assessed using an acidified ferric chloride solution [179]. A significant improvement in crevice corrosion resistance, after a 72 h test, was observed, in particular on active screen treated samples, with a reduction in weight loss of 98% in comparison with the untreated steel. Similar tests were performed on AISI 304L and Ni-free austenitic stainless steels, which were subjected to a carburizing treatment by means of Kolsterizing process [106]. An improvement was registered in crevice corrosion resistance.

3.2.6. Corrosion Phenomena in HCl Solutions

The good corrosion resistance of low-temperature-treated austenitic stainless steels in HCl solutions can also be inferred by the fairly unetched appearance of the modified surface layers in metallographic analysis since HCl is present in many chemical etchants usually used for stainless steels, such as glyceregia and Marble's reagent.

Li and Bell [180] tested the corrosion resistance of AISI 316, which was treated by active screen plasma nitriding at 420 °C for 20 h, in a 10 vol.% HCl water solution for a duration up to 120 h. The weight loss was comparable to that of the untreated steel, but the SEM analysis showed that the dominant corrosion mechanism changed from localized pitting corrosion for the untreated steel to a more general corrosion for the nitrided samples, even if dissolution preferably occurred along slip lines and grain boundaries. A marked increase in the weight loss was observed when a high content of nitrides was able to form, i.e., when the samples were treated at 500 °C. A good corrosion resistance is reported also for carburized stainless steels. Sun [181] tested a carburized cast AISI 316 steel (480 °C, 20 h) in a 2 vol.% HCl solution, and registered a significantly reduction in weight loss up to 6 days when compared to that of the untreated alloy. Potentiodynamic polarization tests showed a higher corrosion resistance of carburized AISI 316L in a 2.5 vol.% HCl solution [182].

3.3. Corrosion Behavior in Presence of Cl-Free Solutions

Austenitic stainless steels have a good corrosion resistance in many environments which do not contain Cl^-. These alloys have a good resistance in very diluted or highly concentrated sulfuric acid (H_2SO_4) solutions, while corrosion occurs more or less easily at intermediate concentrations depending on steel composition. Borate solutions are not usually employed in industrial applications; however, due to their benign character, a stable passive layer can form, and therefore they are commonly used to study the characteristics of this film. Regarding these environments, the corrosion resistance characteristics of the modified surface layers obtained on austenitic stainless steels by means of nitriding or carburizing are summarized in Table 3.

Table 3. Corrosion resistance in Cl-free solutions of the modified surface layers obtained on austenitic stainless steels by means of nitriding or carburizing.

Solution	Modified Layer Type	Nitriding	Carburizing
H_2SO_4	- expanded austenite only	good	good
	- with martensite	poor	-
	- with nitrides (low amount)	poor	-
Na_2SO_4 with/without H_2SO_4	- expanded austenite only	good [1]	-
	- with martensite/nitrides	poor [1]/good [2]	-
Borate	- expanded austenite	good	-

[1] pH 3; [2] pH 6, 9.

3.3.1. Corrosion Behavior in H_2SO_4 and Sulfate Solutions

The study of the corrosion behavior of low-temperature-nitrided austenitic stainless steels in H_2SO_4 solutions is particularly interesting since these surface modified alloys have been proposed as prospective materials for bipolar plates in proton exchange membrane fuel cells (PEMFC) [183–185]. Lin et al. [183] observed typical active–passive behavior with a slight increase in corrosion potential and decrease in corrosion current density for AISI 316 subjected to active screen plasma nitriding (370, 410 and 450 °C, 7 h), when tested in a 0.05 M H_2SO_4 solution, while the anodic current density values in the passive branch tended to be higher than those of the untreated steel. Moreover, higher corrosion resistance was observed in active screen-nitrided (450 °C) specimens, in comparison with the DC plasma-nitrided samples. Tests carried out on plasma-nitrided AISI 316L (370 °C, 2 h) in a H_2SO_4 solution containing 2 ppm F^- (pH = 1–5), used to simulate a PEMFC environment, showed that this sample type had a nobler corrosion potential and lower anodic current density in the passive branch than those of the untreated steel [184]. For pH 1 the corrosion current density of nitrided samples was slightly lower and for pH 2–5 it was comparable to that of the untreated alloy. Further studies on the corrosion behavior of nitrided AISI 316L (450 °C, durations from 3 to 12 h) in a PEFMC environment (0.5 M H_2SO_4 + 2 ppm

HF at 70 °C) showed that the corrosion resistance depended on the phases formed in the modified layers [185]. Both EIS analysis and potentiodynamic polarization tests registered an improvement in the corrosion resistance in comparison with that of the untreated steel. However, as treatment duration was longer and small amounts of nitrides were able to form together with expanded austenite, the corrosion resistance tended to decrease.

The corrosion resistance in H_2SO_4 appears to be especially sensitive to the phases present in the modified layers, and, in particular, to the formation of heterogeneous microstructures. Lei and Zhu [156] studied the corrosion behavior in a 0.05 M H_2SO_4 solution of the expanded austenite with two different N concentrations at the surface, 26 and 32 at.% (steel: 1Cr18Ni9Ti). The potentiodynamic polarization curves of the nitrided samples were comparable to those of the untreated alloy, even if with a slightly higher corrosion resistance, suggesting that the resistance to general corrosion in this environment was equivalent to that of the untreated steel (Figure 13). However, when Lei et al. [158] tested 1Cr18Ni9Ti stainless steel with modified layers consisting of N-rich expanded austenite and expanded austenite + ε_N' in a 0.5 M H_2SO_4 solution, they observed that a single expanded austenite layer had a general corrosion resistance comparable to that of the untreated steel, while the presence of a heterogeneous structure (expanded austenite + N-induced hc.p. martensite) caused an increase in passive current values of 1-2 order of magnitude, which differed from what was observed in a NaCl solution. The precipitation of nitrides decreased the corrosion resistance further on. A similar result was found by Spies et al. [186], who observed that the corrosion resistance in 0.05 M H_2SO_4 depended on nitriding parameters and it was improved only up to a treatment performed at 420 °C for 36 h.

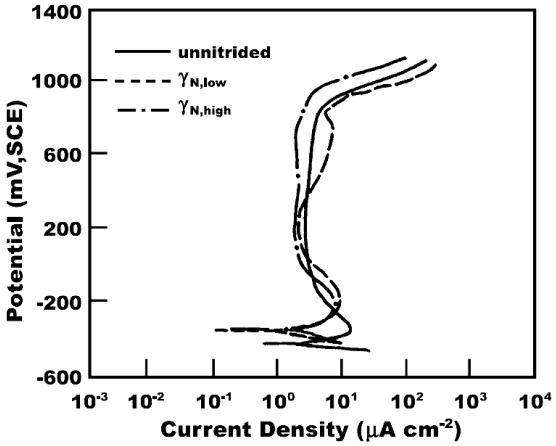

Figure 13. Potentiodynamic polarization curves of 1Cr18Ni9Ti austenitic stainless steel untreated and nitrided with two different N content in expanded austenite ($\gamma_{N,low}$: 26 at.%, $\gamma_{N,high}$: 32 at.%) (solution: 0.05 M H_2SO_4). (For further details, see Ref. [156]). (Reprinted with permission from Ref. [156]. Copyright 2005 Elsevier).

Flis and Gajek [187] tested nitrided AISI 304L steel in a 0.1 M Na_2SO_4 solution acidified with H_2SO_4 to pH 3 by using potentiodynamic method and evaluated the impedance by repeating EIS analysis up to 240 min. All the tests were performed after holding the samples at −1.4 V (MSE) for 2 min, so it has to be hypothesized that at least a part of the passive film formed in the air was destroyed. Using these initial conditions nitrided samples had a higher anodic reactivity than the untreated steel, with a decrease in corrosion resistance. Regarding EIS analysis, using an EEC analogous to that used for electrolyte–polymer–metal system, the authors suggested that the porosity of the film on the nitrided steel was higher than that of the untreated steel. On the basis of steel type, treatment conditions and reported X-ray diffraction patterns, it has to be supposed that N-induced h.c.p. martensite, ε_N', was able to form together with expanded austenite, meaning that the corrosion behavior might be influenced by both a heterogeneous surface layer and a thin passive film, which was not able to properly grow in the probe solution. Further studies showed that when nitrided

AISI 304L (425 °C, 30 h) was put in contact with 0.1 M Na_2SO_4 solution at pH 6 or 9, significantly lower anodic current density values were registered, especially if compared to those of the untreated steel, and a higher corrosion resistance was observed [177].

The influence of N content on the corrosion resistance in a 0.1 M Na_2SO_4 solution acidified to pH 3 was studied by Kuczynska-Wydorska and Flis [188] on nitrided AISI 304L and AISI 316L (425 °C, 30 h). The outer layers, having a higher N concentration (~7–14 wt.%, i.e., ~22–35.7 at.%) and presumably also containing the N-induced h.c.p. martensite and nitrides precipitates due to the nitriding conditions, showed a lower corrosion resistance. Meanwhile, for deeper regions that had a N content less than 7 wt.% (~22 at.%) and presumably consisted of expanded austenite only, the anodic current density values were slightly higher or even lower in the passive and transpassive states in comparison with those of the untreated alloys. An initial acceleration of anodic oxidation was suggested for these samples.

Regarding carburizing, Sun [189] evaluated the corrosion behavior of C-rich expanded austenite formed on AISI 316L steel in a 1 M H_2SO_4 solution. Besides a thin outermost layer, which was due to carbon soot and redeposition of sputtered materials and had a poor electrochemical behavior, the C-rich expanded austenite of the inner part of the modified layer showed an improved corrosion resistance. While the untreated alloy had an active–passive behavior with a clear anodic peak, in the polarization curves of the carburized specimen, related to different depths and thus different C concentrations, very small anodic peaks were observed; moreover, the corrosion potential tended to increase and the corrosion current density tended to decrease as the C content rose. General passivity and transpassivity were not influenced by C concentration and were comparable to those of the untreated alloy. However, in the early stage of potentiostatic polarization experiments a faster film growth kinetic was observed for the carburized samples, and thus it was supposed than there was an enhancement of the initial corrosion resistance in the test solution for this sample type. Carburized AISI 316 showed also a very good corrosion resistance in boiling 16 vol.% H_2SO_4 solution, with a significant reduction in weight loss [190].

The comparison of the corrosion behavior of nitrided (415 °C, 15 h) and carburized (470 °C, 15 h) AISI 316L samples in a 0.5 M H_2SO_4 solution highlighted that the nitrided specimens were more prone to corrosion phenomena, which was probably due to the precipitation of N-induced h.c.p. martensite and/or nitrides, while the carburized samples had a higher corrosion resistance in comparison with that of the untreated steel [191].

3.3.2. Corrosion Behavior in Borate Solutions

A study of the corrosion behavior in a borate buffer solution with pH 8.4 for N-rich expanded austenite, formed on AISI 304L steel, also showed that the modified surface layers maintained good corrosion resistance with these environmental conditions [50]. EIS analysis evidenced higher impedance values and a higher polarization resistance for the nitrided samples than those of the untreated steel. Additionally, in the polarization curves, the nitrided steel had a slightly higher corrosion potential and significantly lower anodic current density values in the passive branch if compared to the untreated alloy. Additional studies, performed in a borate buffer solution with pH increasing from 6.5 to 8.9 [76] and at pH 7.7 [51], also showed that in these conditions N-rich expanded austenite had a stronger tendency to passivation, with an increase in corrosion potential and decrease in anodic current density if compared to the untreated alloy.

4. Conclusions

Low-temperature thermochemical treatments are becoming the treatments of choice for enhancing surface hardness, wear and fatigue resistance without impairing the corrosion resistance of austenitic stainless steels. The main characteristics of the modified surface layers obtained on austenitic stainless steels by means of nitriding or carburizing are summarized in Table 4.

Table 4. Main characteristics of the modified surface layers obtained on austenitic stainless steels by means of nitriding or carburizing.

Properties			Nitriding	Carburizing
Formation temperature (without formation of Cr compounds) (°C)			300–450	300–550
Max. interstitial content in expanded austenite (at.%)			38	19
Max. surface hardness ($kg_f\ mm^{-2}$)			1450	1000
Localized corrosion resistance in Cl^--containing solutions	-	expanded austenite only	very good	good
	-	with martensite	very good-good	-
	-	with nitrides (low amount)	acceptable	-
Corrosion resistance in H_2SO_4 solutions	-	expanded austenite only	good	good
	-	with martensite/nitrides	poor	-
Corrosion resistance in borate buffer solutions	-	expanded austenite	good	-

On the basis of the studies presented in the international literature, the following main conclusions can be drawn.

- The protection effect of expanded austenite and its ability in hindering and delaying the occurrence of corrosion phenomena tend to increase as the interstitial content in this phase is high, the formation of a significant amount of precipitates is avoided and the modified surface layer is thicker. Thus, treatment temperature, duration and N and/or C feeding have to be chosen as functions of the steel composition in order to obtain an interstitial-rich, precipitates-free and thick modified layer.
- Regarding Cl^--containing solutions, both N- and C-rich expanded austenite have improved resistance to localized corrosion (pitting, crevice), delaying or even inhibiting the occurrence of localized corrosion phenomena. The formation of N-induced h.c.p. martensite and/or small amounts of Fe-based nitride precipitates does not impair this resistance. Nitrided samples tested in a 3 wt.% NaCl solution showed an enhanced corrosion resistance in the pH range from 0.4 to 11, with a significant improvement in the pH range 4–11. Carburized samples also showed a good corrosion resistance in NaCl solution at a low pH.
- For nitrided samples, the improvement in corrosion resistance is usually ascribed to the local alkalization of the incipient pits due to the formation of ammonium ions, while for carburized samples the mechanism is still unclear. Taking into account that, in the passive layer, the concentration of both N and C tends to increase in the inner part, where Cr content is usually higher, it may be hypothesized that the preferential Cr-N and Cr-C bonds tend to hinder Cr solubilization and allow to have a more stable and protective film. The change in the semiconductive properties of the film, with a decrease in donor and acceptor density and in the flat band potential value, may also contribute to increasing the protective effect of the passive film.
- In the presence of aqueous environments containing H_2SO_4, the corrosion resistance is comparable or even higher than that of the untreated steel when the modified surface layers consist of expanded austenite only. The corrosion resistance is worse when N-induced h.c.p. martensite and/or Fe-based nitride precipitates are able to form in nitrided samples, or when carbides form in carburized samples. Thus, treatment conditions should be chosen as functions of the steel which are to be treated in order to avoid the formation of a heterogeneous layer at the surface. It has to be pointed out that it is not easy to avoid the formation of h.c.p. martensite in nitrided samples since the solubilization of a high amount of N in expanded austenite induces local plastic deformations, which may be accompanied by the formation of extended stacking faults, i.e., h.c.p. martensite-like zones. On the other hand, modified surface layers, consisting of carbide-free C-rich expanded austenite, can be obtained more easily.

Thus, for applications in H_2SO_4-containing environments, the possible choices seem to be either carburized austenitic stainless steels or nitrided austenitic stainless steels with lower N content than that able to induce the formation of h.c.p. martensite.

- In borate solutions, the good corrosion resistance of austenitic stainless steels is improved further on when N-rich expanded austenite forms.

Thus, the formation of modified surface layers consisting of expanded austenite allows to further extend the applications of austenitic stainless steels. However, a careful choice of the treatment parameters should be made, these being functions of alloy composition, in order to obtain the best performances possible in the service environment.

Funding: This research received no external funding.

Data Availability Statement: Data sharing is not applicable.

Conflicts of Interest: The author declares no conflict of interest.

References

1. Cobb, H.M. *The History of Stainless Steel*; ASM International: Materials Park, OH, USA, 2010; ISBN 978-1-61503-011-8.
2. Washko, S.D.; Aggen, G. Wrought Stainless Steels. In *ASM Handbook Vol. 1*; ASM International: Materials Park, OH, USA, 1997; pp. 841–907.
3. Grubb, J.F.; DeBold, T.; Fritz, J.D. Corrosion of Wrought Stainless Steels. In *ASM Handbook Vol. 13B*; Cramer, S.D., Covino, B.S., Jr., Eds.; ASM International: Materials Park, OH, USA, 2005; pp. 54–77. [CrossRef]
4. Sun, J.; Tang, H.; Wang, C.; Han, Z.; Li, S. Effects of Alloying Elements and Microstructure on Stainless Steel Corrosion: A Review. *Steel Res. Int.* **2022**, *93*, 2100450. [CrossRef]
5. Asami, K.; Hashimoto, K. Importance of initial surface film in the degradation of stainless steels by atmospheric exposure. *Corros. Sci.* **2003**, *45*, 2263–2283. [CrossRef]
6. Habibzadeh, S.; Li, L.; Shum-Tim, D.; Davis, E.C.; Omanovic, S. Electrochemical polishing as a 316L stainless steel surface treatment method: Towards the improvement of biocompatibility. *Corros. Sci.* **2014**, *87*, 89–100. [CrossRef]
7. Łyczkowska-Widłak, E.; Lochyński, P.; Nawrat, G. Electrochemical Polishing of Austenitic Stainless Steels. *Materials* **2020**, *13*, 2557. [CrossRef] [PubMed]
8. Olsson, C.O.A.; Landolt, D. Passive films on stainless steels-Chemistry, structure and growth. *Electrochim. Acta* **2003**, *48*, 1093–1104. [CrossRef]
9. Jiang, R.; Wang, Y.; Wen, X.; Chen, C.; Zhao, J. Effect of time on the characteristics of passive film formed on stainless steel. *Appl. Surf. Sci.* **2017**, *412*, 214–222. [CrossRef]
10. McGuire, M.F. *Stainless Steels for Design Engineers*; ASM International: Materials Park, OH, USA, 2008; ISBN 978-0-87170-717-8.
11. Saadi, S.A.; Yi, Y.; Cho, P.; Jang, C.; Beeley, P. Passivity breakdown of 316L stainless steel during potentiodynamic polarization in NaCl solution. *Corros. Sci.* **2016**, *111*, 720–727. [CrossRef]
12. Wang, Z.; Seyeux, A.; Zanna, S.; Maurice, V.; Marcus, P. Chloride-induced alterations of the passive film on 316L stainless steel and blocking effect of pre-passivation. *Electrochim. Acta* **2020**, *329*, 135159. [CrossRef]
13. Astafurov, S.; Astafurova, E. Phase Composition of Austenitic Stainless Steels in Additive Manufacturing: A Review. *Metals* **2021**, *11*, 1052. [CrossRef]
14. Schneider, M.J.; Chatterjee, M.S. Introduction to Surface Hardening of Steels. In *ASM Handbook Vol. 4A*; Dosset, J.L., Totten, G.E., Eds.; ASM International: Materials Park, OH, USA, 2013; pp. 389–397. [CrossRef]
15. Davis, J.R. Surface Engineering of Stainless Steels. In *ASM Metal Handbook Vol. 5*; ASM International: Materials Park, OH, USA, 1994; pp. 741–761. [CrossRef]
16. Michal, G.M.; Gu, X.; Jennings, W.D.; Kahn, H.; Ernst, F.; Heuer, A.H. Paraequilibrium Carburization of Duplex and Ferritic Stainless Steels. *Metall. Mater. Trans. A* **2009**, *40*, 1781–1790. [CrossRef]
17. Adachi, S.; Ueda, N. Formation of Expanded Austenite on a Cold-Sprayed AISI 316L Coating by Low-Temperature Plasma Nitriding. *J. Therm. Spray Technol.* **2015**, *24*, 1399–1407. [CrossRef]
18. Adachi, S.; Yamaguchi, T.; Ueda, N. Formation and Properties of Nitrocarburizing S-Phase on AISI 316L Stainless Steel-Based WC Composite Layers by Low-Temperature Plasma Nitriding. *Metals* **2021**, *11*, 1538. [CrossRef]
19. Lindner, T.; Kutschmann, P.; Löbel, M.; Lampke, T. Hardening of HVOF-Sprayed Austenitic Stainless-Steel Coatings by Gas Nitriding. *Coatings* **2018**, *8*, 348. [CrossRef]
20. Lindner, T.; Löbel, M.; Lampke, T. Phase Stability and Microstructure Evolution of Solution-Hardened 316L Powder Feedstock for Thermal Spraying. *Metals* **2018**, *8*, 1063. [CrossRef]
21. Qadri, S.A.R.; Sasidhar, K.N.; Meka, S.R. High nitrogen alloying of AISI 316 L stainless steel powder by nitriding. *Powder Technol.* **2021**, *390*, 456–463. [CrossRef]
22. Dong, H. S-phase surface engineering of Fe-Cr, Co-Cr and Ni-Cr alloys. *Int. Mater. Rev.* **2010**, *55*, 65–98. [CrossRef]

23. Christiansen, T.L.; Somers, M.A.J. Low-temperature gaseous surface hardening of stainless steel: The current status. *Int. J. Mater. Res.* **2009**, *100*, 1361–1377. [CrossRef]
24. Borgioli, F. From Austenitic Stainless Steel to Expanded Austenite-S Phase: Formation, Characteristics and Properties of an Elusive Metastable Phase. *Metals* **2020**, *10*, 187. [CrossRef]
25. Collins, S.R.; Williams, P.C.; Marx, S.V.; Heuer, A.; Ernst, F.; Kahn, H. Low-Temperature Carburization of Austenitic Stainless Steels. In *ASM Handbook Vol. 4D*; Dosset, J., Totten, G.E., Eds.; ASM International: Materials Park, OH, USA, 2014; pp. 451–460.
26. Casteletti, L.C.; Neto, A.L.; Totten, G.E. Nitriding of Stainless Steels. *Metallogr. Microstruct. Anal.* **2014**, *3*, 477–508. [CrossRef]
27. Bell, T. Surface engineering of austenitic stainless steel. *Surf. Eng.* **2002**, *18*, 415–422. [CrossRef]
28. Czerwiec, T.; He, H.; Marcos, G.; Thiriet, T.; Weber, S.; Michel, H. Fundamental and Innovations in Plasma Assisted Diffusion of Nitrogen and Carbon in Austenitic Stainless Steels and Related Alloys. *Plasma Process. Polym.* **2009**, *6*, 401–409. [CrossRef]
29. Somers, M.A.J.; Christiansen, T.L. Low temperature surface hardening of stainless steel. In *Thermochemical Surface Engineering of Steels*; Mittemeijer, E.J., Somers, M.A.J., Eds.; Woodhead Publishing: Oxford, UK, 2015; pp. 557–579. ISBN 978-0-85709-592-3. [CrossRef]
30. Fossati, A.; Galvanetto, E.; Bacci, T.; Borgioli, F. Improvement of corrosion resistance of austenitic stainless steels by means of glow-discharge nitriding. *Corros. Rev.* **2011**, *29*, 209–221. [CrossRef]
31. Luo, Q.; Yang, S. From Micro to Nano Scales -Recent Progress in the Characterization of Nitrided Austenitic Stainless Steels. *Int. J. Nanomed. Nanosurgery* **2015**, *1*, 1–11. [CrossRef]
32. Somers, M.; Kücükyildiz, Ö.; Ormstrup, C.; Alimadadi, H.; Hattel, J.; Christiansen, T.; Winther, G. Residual Stress in Expanded Austenite on Stainless Steel; Origin, Measurement, and Prediction. *Mater. Perform. Charact.* **2018**, *7*, 693–716. [CrossRef]
33. Borgioli, F. The "Expanded" Phases in the Low-Temperature Treated Stainless Steels: A Review. *Metals* **2022**, *12*, 331. [CrossRef]
34. Cardoso, R.P.; Mafra, M.; Brunatto, S.F. Low-temperature Thermochemical Treatments of Stainless Steels–An Introduction. In *Plasma Science and Technology-Progress in Physical States and Chemical Reactions*; Mieso, T., Ed.; InTech: Rijeka, Croatia, 2016; pp. 107–130. ISBN 978-953-51-2280-7. [CrossRef]
35. Tschiptschin, A.P.; Pinedo, C.E. Surface Hardening of Stainless Steel. In *Stainless Steels*; Singh, A., Ed.; IntechOpen: Rijeka, Croatia, 2022; pp. 94–174. ISBN 978-1-80355-133-3. [CrossRef]
36. Spies, H.-J. Corrosion behaviour of nitrided, nitrocarburised and carburised steels. In *Thermochemical Surface Engineering of Steel*; Mittemeijer, E.J., Somers, M.A.J., Eds.; Woodhead Publishing: Oxford, UK, 2015; pp. 267–309. ISBN 978-0-85709-592-3. [CrossRef]
37. Wriedt, H.A.; Gokcen, N.A.; Nafziger, R.H. The Fe-N (Iron-Nitrogen) system. *Bull. Alloy Phase Diagr.* **1987**, *8*, 355–377. [CrossRef]
38. Okamoto, H. The C-Fe (carbon-iron) system. *J. Phase Equilibria* **1992**, *13*, 543–565. [CrossRef]
39. Gavriljuk, V.G. Carbon and nitrogen in iron-based austenite and martensite: An attempt at comparative analysis. *J. Phys. IV Fr.* **2003**, *112*, 51–59. [CrossRef]
40. Cao, Y.; Ernst, F.; Michal, G.M. Colossal carbon supersaturation in austenitic stainless steels carburized at low temperature. *Acta Mater.* **2003**, *51*, 4171–4181. [CrossRef]
41. Williamson, D.L.; Ozturk, O.; Wei, R.; Wilbur, P.J. Metastable phase formation and enhanced diffusion in f.c.c. alloys under high dose, high flux nitrogen implantation at high and low ion energies. *Surf. Coat. Technol.* **1994**, *65*, 15–23. [CrossRef]
42. Christiansen, T.; Somers, M.A.J. Controlled dissolution of colossal quantities of nitrogen in stainless steel. *Metall. Mater. Trans. A* **2006**, *37*, 675–682. [CrossRef]
43. Christiansen, T.L.; Ståhl, K.; Brink, B.K.; Somers, M.A.J. On the Carbon Solubility in Expanded Austenite and Formation of Hägg Carbide in AISI 316 Stainless Steel. *Steel Res. Int.* **2016**, *87*, 1395–1405. [CrossRef]
44. Schmuki, P. From Bacon to barriers: A review on the passivity of metals and alloys. *J. Solid State Electrochem.* **2002**, *6*, 145–164. [CrossRef]
45. Wang, Z.; Paschalidou, E.-M.; Seyeux, A.; Zanna, S.; Maurice, V.; Marcus, P. Mechanisms of Cr and Mo Enrichments in the Passive Oxide Film on 316L Austenitic Stainless Steel. *Front. Mater.* **2019**, *6*, 232. [CrossRef]
46. Hakiki, N.B.; Boudin, S.; Rondot, B.; Da Cunha Belo, M. The electronic structure of passive films formed on stainless steels. *Corros. Sci.* **1995**, *37*, 1809–1822. [CrossRef]
47. Maurice, V.; Marcus, P. Progress in corrosion science at atomic and nanometric scales. *Prog. Mater. Sci.* **2018**, *95*, 132–171. [CrossRef]
48. Maurice, V.; Marcus, P. Current developments of nanoscale insight into corrosion protection by passive oxide films. *Curr. Opin. Solid State Mater. Sci.* **2018**, *22*, 156–167. [CrossRef]
49. Lei, M.K.; Zhu, X.M. Role of Nitrogen in Pitting Corrosion Resistance of a High-Nitrogen Face-Centered-Cubic Phase Formed on Austenitic Stainless Steel. *J. Electrochem. Soc.* **2005**, *152*, B291–B295. [CrossRef]
50. Wang, K.S.; Tong, S.; Lei, M.K. Corrosion and Passivation of High Nitrogen Face-Centered-Cubic Phase Formed on AISI 304L Austenitic Stainless Steel in Borate Buffer Solution. *J. Electrochem. Soc.* **2015**, *162*, C601–C609. [CrossRef]
51. Tong, S.; Che, H.L.; Lei, M.K. High-resolution TEM characterization of epitaxial passivation for a high nitrogen face-centered-cubic phase formed on AISI 304L austenitic stainless steel in borate buffer solution. *Electrochim. Acta* **2021**, *393*, 139075. [CrossRef]
52. Heuer, A.H.; Kahn, H.; Ernst, F.; Michal, G.M.; Hovis, D.B.; Rayne, R.J.; Martin, F.J.; Natishan, P.M. Enhanced corrosion resistance of interstitially hardened stainless steel: Implications of a critical passive layer thickness for breakdown. *Acta Mater.* **2012**, *60*, 716–725. [CrossRef]

53. Ningshen, S.; Mudali, U.K.; Mittal, V.K.; Khatak, H.S. Semiconducting and passive film properties of nitrogen-containing type 316LN stainless steels. *Corros. Sci.* **2007**, *49*, 481–496. [CrossRef]
54. Zhu, X.M.; Guo, Y.; Xing, Z.Q.; Lei, M.K. Effect of Nitrogen on Semiconducting Properties of Passive Films of a High Nitrogen Face-Centered-Cubic Phase Formed on Austenitic Stainless Steel. *J. Electrochem. Soc.* **2012**, *159*, C319–C325. [CrossRef]
55. Sun, Y. Corrosion behaviour of low temperature plasma carburised 316L stainless steel in chloride containing solutions. *Corros. Sci.* **2010**, *52*, 2661–2670. [CrossRef]
56. Liu, H.Y.; Che, H.L.; Gao, J.Y.; Li, G.B.; Lei, M.K. Low-pressure hollow cathode plasma source carburizing of AISI 304L austenitic stainless steel at low temperature. *Surf. Coat. Technol.* **2022**, *442*, 128548. [CrossRef]
57. Paredes, E.C.; Bautista, A.; Alvarez, S.M.; Velasco, F. Influence of the forming process of corrugated stainless steels on their corrosion behaviour in simulated pore solutions. *Corros. Sci.* **2012**, *58*, 52–61. [CrossRef]
58. Cheng, Y.F.; Luo, J.L. Electronic structure and pitting susceptibility of passive film on carbon steel. *Electrochim. Acta* **1999**, *44*, 2947–2957. [CrossRef]
59. Hänninen, H.; Romu, J.; Ilola, R.; Tervo, J.; Laitinen, A. Effects of processing and manufacturing of high nitrogen-containing stainless steels on their mechanical, corrosion and wear properties. *J. Mater. Process. Technol.* **2001**, *117*, 424–430. [CrossRef]
60. Lo, K.H.; Shek, C.H.; Lai, J.K.L. Recent developments in stainless steels. *Mater. Sci. Eng. R Rep.* **2009**, *65*, 39–104. [CrossRef]
61. Sumita, M.; Hanawa, T.; Teoh, S.H. Development of nitrogen-containing nickel-free austenitic stainless steels for metallic biomaterials—Review. *Mater. Sci. Eng. C* **2004**, *24*, 753–760. [CrossRef]
62. Chen, S.; Wang, Q.; Yang, H.; Yang, K. High-Nitrogen Nickel-Free Stainless Steel: An Attractive Material with Potential for Biomedical Application. *Steel Res. Int.* **2022**, 2200355. [CrossRef]
63. Baba, H.; Kodama, T.; Katada, Y. Role of nitrogen on the corrosion behavior of austenitic stainless steels. *Corros. Sci.* **2002**, *44*, 2393–2407. [CrossRef]
64. Speidel, M.O. Corrosion Science of Stainless Steels. In *Stainless Steels '91. Proceedings of the International Conference on Stainless Steels, Chiba, Japan, 10–13 June 1991*; Iron and Steel Institute of Japan: Tokyo, Japan, 1991; Volume 1, pp. 25–35.
65. Jargelius-Pettersson, R.F.A. Electrochemical investigation of the influence of nitrogen alloying on pitting corrosion of austenitic stainless steels. *Corros. Sci.* **1999**, *41*, 1639–1664. [CrossRef]
66. Baba, H.; Katada, Y. Effect of nitrogen on crevice corrosion in austenitic stainless steel. *Corros. Sci.* **2006**, *48*, 2510–2524. [CrossRef]
67. Olefjord, I.; Wegrelius, L. The influence of nitrogen on the passivation of stainless steels. *Corros. Sci.* **1996**, *38*, 1203–1220. [CrossRef]
68. Vehovar, L.; Vehovar, A.; Metikoš-Huković, M.; Tandler, M. Investigations into the stress corrosion cracking of stainless steel alloyed with nitrogen. *Mater. Corros.* **2002**, *53*, 316–327. [CrossRef]
69. Kadowaki, M.; Saengdeejing, A.; Muto, I.; Chen, Y.; Frankel, G.S.; Doi, T.; Kawano, K.; Sugawara, Y.; Hara, N. Roles of Interstitial Nitrogen, Carbon, and Boron in Steel Corrosion: Generation of Oxyanions and Stabilization of Electronic Structure. *J. Electrochem. Soc.* **2020**, *167*, 81503. [CrossRef]
70. Baba, H.; Katada, Y. Effect of Nitrogen on Crevice Corrosion and Repassivation Behavior of Austenitic Stainless Steel. *Mater. Trans.* **2008**, *49*, 579–586. [CrossRef]
71. Ives, M.B.; Lu, Y.C.; Luo, J.L. Cathodic reactions involved in metallic corrosion in chlorinated saline environments. *Corros. Sci.* **1991**, *32*, 91–102. [CrossRef]
72. Clayton, C.R.; Rosenzweig, L.; Oversluizen, M.; Lu, Y.C. The influence of nitrogen on the passivity of 18-8 (0.24%N) stainless steels. In *Surfaces, Inhibition and Passivation*; McCafferty, E., Brodd, R.J., Eds.; The Electrochemical Society: Pennington, NJ, USA, 1986; pp. 323–339.
73. Bayoumi, F.M.; Ghanem, W.A. Effect of nitrogen on the corrosion behavior of austenitic stainless steel in chloride solutions. *Mater. Lett.* **2005**, *59*, 3311–3314. [CrossRef]
74. Zhu, X.M.; Lei, M.K. Pitting corrosion resistance of high nitrogen f.c.c. phase in plasma source ion nitrided austenitic stainless steel. *Surf. Coat. Technol.* **2000**, *131*, 400–403. [CrossRef]
75. Flis-Kabulska, I.; Sun, Y.; Flis, J. Monitoring the near-surface pH to probe the role of nitrogen in corrosion behaviour of low-temperature plasma nitrided 316L stainless steel. *Electrochim. Acta* **2013**, *104*, 208–215. [CrossRef]
76. Tong, S.; Che, H.L.; Wang, K.S.; Lei, M.K. Passivation kinetics of a high nitrogen face-centered-cubic phase formed on AISI 304L austenitic stainless steel in borate buffer solutions by photo- and electrochemical methods. *Electrochim. Acta* **2021**, *394*, 139110. [CrossRef]
77. Metikoš-Huković, M.; Babić, R.; Grubač, Z.; Petrović, Ž.; Lajçi, N. High corrosion resistance of austenitic stainless steel alloyed with nitrogen in an acid solution. *Corros. Sci.* **2011**, *53*, 2176–2183. [CrossRef]
78. Sun, S.; Wei, S.; Wang, G.; Jiang, Z.; Lian, J.; Ji, C. The Synthesis and Electrochemical Behavior of High-Nitrogen Nickel-Free Austenitic Stainless Steel. *J. Mater. Eng. Perform.* **2014**, *23*, 3957–3962. [CrossRef]
79. Wu, X.Q.; Xu, S.; Huang, J.B.; Han, E.H.; Ke, W.; Yang, K.; Jiang, Z.H. Uniform corrosion and intergranular corrosion behavior of nickel-free and manganese alloyed high nitrogen stainless steels. *Mater. Corros.* **2008**, *59*, 676–684. [CrossRef]
80. Martin, F.J.; Lemieux, E.J.; Newbauer, T.M.; Bayles, R.A.; Natishan, P.M.; Kahn, H.; Michal, G.M.; Ernst, F.; Heuer, A.H. Carburization-induced passivity of 316 L austenitic stainless steel. *Electrochem. Solid-State Lett.* **2007**, *10*, C76–C78. [CrossRef]
81. Niu, W.; Lillard, R.S.; Li, Z.; Ernst, F. Properties of the Passive Film Formed on Interstitially Hardened AISI 316L Stainless Steel. *Electrochim. Acta* **2015**, *176*, 410–419. [CrossRef]

82. Li, T.; Chien, S.-C.; Ren, Z.; Windl, W.; Ernst, F.; Frankel, G.S. Understanding the efficacy of concentrated interstitial carbon in enhancing the pitting corrosion resistance of stainless steel. *Acta Mater.* **2021**, *221*, 117433. [CrossRef]
83. Borgioli, F.; Fossati, A.; Galvanetto, E.; Bacci, T. Glow-discharge nitriding of AISI 316L austenitic stainless steel: Influence of treatment temperature. *Surf. Coat. Technol.* **2005**, *200*, 2474–2480. [CrossRef]
84. Borgioli, F.; Fossati, A.; Galvanetto, E.; Bacci, T.; Pradelli, G. Glow discharge nitriding of AISI 316L austenitic stainless steel: Influence of treatment pressure. *Surf. Coat. Technol.* **2006**, *200*, 5505–5513. [CrossRef]
85. Borgioli, F.; Galvanetto, E.; Bacci, T. Influence of surface morphology and roughness on water wetting properties of low temperature nitrided austenitic stainless steels. *Mater. Charact.* **2014**, *95*, 278–284. [CrossRef]
86. Stinville, J.C.; Cormier, J.; Templier, C.; Villechaise, P. Modeling of the lattice rotations induced by plasma nitriding of 316L polycrystalline stainless steel. *Acta Mater.* **2015**, *83*, 10–16. [CrossRef]
87. Czerwiec, T.; Tsareva, S.; Andrieux, A.; Bruyère, S.; Marcos, G. Effects of surface topography at different scales on the dispersion of the wetting data for sessile water droplets on nitrided austenitic stainless steels. *Surf. Coat. Technol.* **2022**, *441*, 128510. [CrossRef]
88. Tao, X.; Liu, X.; Matthews, A.; Leyland, A. The influence of stacking fault energy on plasticity mechanisms in triode-plasma nitrided austenitic stainless steels: Implications for the structure and stability of nitrogen-expanded austenite. *Acta Mater.* **2019**, *164*, 60–75. [CrossRef]
89. Baranowska, J.; Arnold, B. Corrosion resistance of nitrided layers on austenitic steel. *Surf. Coat. Technol.* **2006**, *200*, 6623–6628. [CrossRef]
90. Bottoli, F.; Jellesen, M.S.; Christiansen, T.L.; Winther, G.; Somers, M.A.J. High temperature solution-nitriding and low-temperature nitriding of AISI 316: Effect on pitting potential and crevice corrosion performance. *Appl. Surf. Sci.* **2018**, *431*, 24–31. [CrossRef]
91. Farrell, K.; Specht, E.D.; Pang, J.; Walker, L.R.; Rar, A.; Mayotte, J.R. Characterization of a carburized surface layer on an austenitic stainless steel. *J. Nucl. Mater.* **2005**, *343*, 123–133. [CrossRef]
92. Gallo, S.C.; Dong, H. EBSD and AFM observations of the microstructural changes induced by low temperature plasma carburising on AISI 316. *Appl. Surf. Sci.* **2011**, *258*, 608–613. [CrossRef]
93. Maistro, G.; Yao, Y.; Klement, U.; Nyborg, L.; Cao, Y. On surface carbides in low-temperature carburized austenitic stainless steels. *Mater. Charact.* **2020**, *167*, 110462. [CrossRef]
94. Cisquini, P.; Ramos, S.V.; Viana, P.R.P.; Lins, V.d.F.C.; Franco, A.R.; Vieira, E.A. Effect of the roughness produced by plasma nitrocarburizing on corrosion resistance of AISI 304 austenitic stainless steel. *J. Mater. Res. Technol.* **2019**, *8*, 1897–1906. [CrossRef]
95. Borgioli, F.; Galvanetto, E.; Bacci, T. Corrosion behaviour of low temperature nitrided nickel-free, AISI 200 and AISI 300 series austenitic stainless steels in NaCl solution. *Corros. Sci.* **2018**, *136*, 352–365. [CrossRef]
96. De Las Heras, E.; Ybarra, G.; Lamas, D.; Cabo, A.; Dalibon, E.L.; Brühl, S.P. Plasma nitriding of 316L stainless steel in two different N_2-H_2 atmospheres-Influence on microstructure and corrosion resistance. *Surf. Coat. Technol.* **2017**, *313*, 47–54. [CrossRef]
97. Li, G.Y.; Lei, M.K. Microstructure and Properties of Plasma Source Nitrided AISI 316 Austenitic Stainless Steel. *J. Mater. Eng. Perform.* **2017**, *26*, 418–423. [CrossRef]
98. Williamson, D.L.; Davis, J.A.; Wilbur, P.J. Effect of austenitic stainless steel composition on low-energy, high-flux, nitrogen ion beam processing. *Surf. Coat. Technol.* **1998**, *103*, 178–184. [CrossRef]
99. Borgioli, F.; Galvanetto, E.; Bacci, T. Low temperature nitriding of AISI 300 and 200 series austenitic stainless steels. *Vacuum* **2016**, *127*, 51–60. [CrossRef]
100. Czerwiec, T.; Renevier, N.; Michel, H. Low-temperature plasma-assisted nitriding. *Surf. Coat. Technol.* **2000**, *131*, 267–277. [CrossRef]
101. Czerwiec, T.; He, H.; Weber, S.; Dong, C.; Michel, H. On the occurrence of dual diffusion layers during plasma-assisted nitriding of austenitic stainless steel. *Surf. Coat. Technol.* **2006**, *200*, 5289–5295. [CrossRef]
102. Christiansen, T.; Dahl, K.V.; Somers, M.A.J. Nitrogen diffusion and nitrogen depth profiles in expanded austenite: Experimental assessment, numerical simulation and role of stress. *Mater. Sci. Technol.* **2008**, *24*, 159–167. [CrossRef]
103. Michler, T. Influence of plasma nitriding on hydrogen environment embrittlement of 1.4301 austenitic stainless steel. *Surf. Coat. Technol.* **2008**, *202*, 1688–1695. [CrossRef]
104. Sun, Y. Hybrid plasma surface alloying of austenitic stainless steels with nitrogen and carbon. *Mater. Sci. Eng. A* **2005**, *404*, 124–129. [CrossRef]
105. Christiansen, T.; Somers, M.A.J. Low temperature gaseous nitriding and carburising of stainless steel. *Surf. Eng.* **2005**, *21*, 445–455. [CrossRef]
106. Formosa, D.; Hunger, R.; Spiteri, A.; Dong, H.; Sinagra, E.; Buhagiar, J. Corrosion behaviour of carbon S-phase created on Ni-free biomedical stainless steel. *Surf. Coat. Technol.* **2012**, *206*, 3479–3487. [CrossRef]
107. Werner, K.V.; Che, H.L.; Lei, M.K.; Christiansen, T.L.; Somers, M.A.J. Low Temperature Carburizing of Stainless Steels and the Development of Carbon Expanded Austenite. *HTM J. Heat Treat. Mater.* **2022**, *77*, 3–15. [CrossRef]
108. Borgioli, F.; Fossati, A.; Matassini, G.; Galvanetto, E.; Bacci, T. Low temperature glow-discharge nitriding of a low nickel austenitic stainless steel. *Surf. Coat. Technol.* **2010**, *204*, 3410–3417. [CrossRef]
109. Fewell, M.P.; Priest, J.M. High-order diffractometry of expanded austenite using synchrotron radiation. *Surf. Coat. Technol.* **2008**, *202*, 1802–1815. [CrossRef]

110. Zhidkov, I.S.; Kukharenko, A.I.; Makarov, A.V.; Savrai, R.A.; Gavrilov, N.V.; Cholakh, S.O.; Kurmaev, E.Z. XPS characterization of surface layers of stainless steel nitrided in electron beam plasma at low temperature. *Surf. Coat. Technol.* **2020**, *386*, 125492. [CrossRef]
111. Martinavičius, A.; Abrasonis, G.; Scheinost, A.C.; Danoix, R.; Danoix, F.; Stinville, J.C.; Talut, G.; Templier, C.; Liedke, O.; Gemming, S.; et al. Nitrogen interstitial diffusion induced decomposition in AISI 304L austenitic stainless steel. *Acta Mater.* **2012**, *60*, 4065–4076. [CrossRef]
112. Oddershede, J.; Christiansen, T.L.; Ståhl, K.; Somers, M.A.J. Extended X-ray absorption fine structure investigation of nitrogen stabilized expanded austenite. *Scr. Mater.* **2010**, *62*, 290–293. [CrossRef]
113. Che, H.L.; Tong, S.; Wang, K.S.; Lei, M.K.; Somers, M.A.J. Co-existence of γ_N′ phase and γ_N phase on nitrided austenitic Fe–Cr–Ni alloys- I. experiment. *Acta Mater.* **2019**, *177*, 35–45. [CrossRef]
114. Che, H.L.; Lei, M.K. Microstructure of perfect nitrogen-expanded austenite formed by unconstrained nitriding. *Scr. Mater.* **2021**, *194*, 113705. [CrossRef]
115. Che, H.L.; Lei, M.K.; Somers, M.A.J. A simple model for nitrogen-induced lattice expansion of γ_N′ and γN phases in Fe–Cr–Ni alloys with different chromium contents. *Philos. Mag. Lett.* **2020**, *100*, 435–441. [CrossRef]
116. Che, H.L.; Christiansen, T.L.; Lei, M.K.; Somers, M.A.J. Co-existence of γ_N′ phase and γ_N phase in nitrided austenitic Fe-Cr-Ni alloys-II: A pragmatic modeling approach. *Acta Mater.* **2022**, *235*, 118094. [CrossRef]
117. Lei, M.K. Phase transformations in plasma source ion nitrided austenitic stainless steel at low temperature. *J. Mater. Sci.* **1999**, *34*, 5975–5982. [CrossRef]
118. Tao, X.; Qi, J.; Rainforth, M.; Matthews, A.; Leyland, A. On the interstitial induced lattice inhomogeneities in nitrogen-expanded austenite. *Scr. Mater.* **2020**, *185*, 146–151. [CrossRef]
119. Tong, K.; Ye, F.; Che, H.; Lei, M.K.; Miao, S.; Zhang, C. High-density stacking faults in a supersaturated nitrided layer on austenitic stainless steel. *J. Appl. Crystallogr.* **2016**, *49*, 1967–1971. [CrossRef]
120. Lei, M.K.; Huang, Y.; Zhang, Z.L. In situ Transformation of Nitrogen-induced h.c.p. Martensite in Plasma Source Ion–nitrided Austenitic Stainless Steel. *J. Mater. Sci. Lett.* **1998**, *17*, 1165–1167. [CrossRef]
121. Sah, J.V.; Dwivedi, P.K.; Mukherjee, S.; Jhala, G.; Joseph, A. Influence of γ_N′ and ε_N′ phases on the properties of AISI 304L after low-temperature plasma nitrocarburizing. *J. Vac. Sci. Technol. A* **2023**, *41*, 33101. [CrossRef]
122. Sah, J.; Joseph, A.; Jhala, G.; Mukherjee, S. On the Effects of H2 and Ar on Dual Layer Formed by Plasma Nitrocarburizing on Austenitic Stainless Steels. *J. Mater. Eng. Perform.* **2022**, *31*, 2664–2677. [CrossRef]
123. Borgioli, F.; Galvanetto, E.; Bacci, T. Surface Modification of a Nickel-Free Austenitic Stainless Steel by Low-Temperature Nitriding. *Metals* **2021**, *11*, 1845. [CrossRef]
124. Borgioli, F.; Galvanetto, E.; Bacci, T. Effects of surface modification by means of low temperature plasma nitriding on wetting and corrosion behavior of austenitic stainless steel. *Coatings* **2020**, *10*, 98. [CrossRef]
125. Borgioli, F.; Galvanetto, E.; Bacci, T. Surface modification of austenitic stainless steel by means of low pressure glow-discharge treatments with nitrogen. *Coatings* **2019**, *9*, 604. [CrossRef]
126. Tsujikawa, M.; Yamauchi, N.; Ueda, N.; Sone, T.; Hirose, Y. Behavior of carbon in low temperature plasma nitriding layer of austenitic stainless steel. *Surf. Coat. Technol.* **2005**, *193*, 309–313. [CrossRef]
127. Manova, D.; Mändl, S. Initial phase formation during nitriding of austenitic stainless steel. *Surf. Coat. Technol.* **2023**, *456*, 129258. [CrossRef]
128. Collins, G.A.; Hutchings, R.; Short, K.T.; Tendys, J.; Li, X.; Samandi, M. Nitriding of austenitic stainless steel by plasma immersion ion implantation. *Surf. Coat. Technol.* **1995**, *74*, 417–424. [CrossRef]
129. Borgioli, F.; Fossati, A.; Raugei, L.; Galvanetto, E.; Bacci, T. Low temperature glow-discharge nitriding of stainless steels. In Proceedings of the 7th European Stainless Steel Conference: Science and Market, Como, Italy, 21–23 September 2011; Associazione Italiana di Metallurgia: Milan, Italy, 2011.
130. Tao, X.; Li, X.; Dong, H.; Matthews, A.; Leyland, A. Evaluation of the sliding wear and corrosion performance of triode-plasma nitrided Fe-17Cr-20Mn-0.5N high-manganese and Fe-19Cr-35Ni-1.2Si high-nickel austenitic stainless steels. *Surf. Coat. Technol.* **2021**, *409*, 126890. [CrossRef]
131. Fossati, A.; Borgioli, F.; Galvanetto, E.; Bacci, T. Glow-discharge nitriding of AISI 316L austenitic stainless steel: Influence of treatment time. *Surf. Coat. Technol.* **2006**, *200*, 3511–3517. [CrossRef]
132. Wu, D.; Ge, Y.; Kahn, H.; Ernst, F.; Heuer, A.H. Diffusion profiles after nitrocarburizing austenitic stainless steel. *Surf. Coat. Technol.* **2015**, *279*, 180–185. [CrossRef]
133. Sun, Y.; Li, X.; Bell, T. Low temperature plasma carburising of austenitic stainless steels for improved wear and corrosion resistance. *Surf. Eng.* **1999**, *15*, 49–54. [CrossRef]
134. Revilla, R.I.; Wouters, B.; Andreatta, F.; Lanzutti, A.; Fedrizzi, L.; De Graeve, I. EIS comparative study and critical Equivalent Electrical Circuit (EEC) analysis of the native oxide layer of additive manufactured and wrought 316L stainless steel. *Corros. Sci.* **2020**, *167*, 108480. [CrossRef]
135. Marcelin, S.; Pébère, N.; Régnier, S. Electrochemical characterisation of a martensitic stainless steel in a neutral chloride solution. *Electrochim. Acta* **2013**, *87*, 32–40. [CrossRef]
136. Omanovic, S.; Roscoe, S.G. Electrochemical Studies of the Adsorption Behavior of Bovine Serum Albumin on Stainless Steel. *Langmuir* **1999**, *15*, 8315–8321. [CrossRef]

137. Perumal, G.; Grewal, H.S.; Arora, H.S. Enhanced durability, bio-activity and corrosion resistance of stainless steel through severe surface deformation. *Colloids Surf. B Biointerfaces* **2020**, *194*, 111197. [CrossRef] [PubMed]
138. Bou-Saleh, Z.; Shahryari, A.; Omanovic, S. Enhancement of corrosion resistance of a biomedical grade 316LVM stainless steel by potentiodynamic cyclic polarization. *Thin Solid Film.* **2007**, *515*, 4727–4737. [CrossRef]
139. Harrington, D.A.; van den Driessche, P. Mechanism and equivalent circuits in electrochemical impedance spectroscopy. *Electrochim. Acta* **2011**, *56*, 8005–8013. [CrossRef]
140. Tandon, V.; Patil, A.P. On the Influence of Cold Working and Electrochemical Nitridation on the Corrosion Behaviour of 316L Austenitic Stainless Steel in Acidic Environment. *Surf. Eng. Appl. Electrochem.* **2020**, *56*, 63–70. [CrossRef]
141. Sheng, X.; Ting, Y.P.; Pehkonen, S.O. The influence of sulphate-reducing bacteria biofilm on the corrosion of stainless steel AISI 316. *Corros. Sci.* **2007**, *49*, 2159–2176. [CrossRef]
142. Wang, L.; Tian, H.; Gao, H.; Xie, F.; Zhao, K.; Cui, Z. Electrochemical and XPS analytical investigation of the accelerative effect of bicarbonate/carbonate ions on AISI 304 in alkaline environment. *Appl. Surf. Sci.* **2019**, *492*, 792–807. [CrossRef]
143. Shahryari, A.; Omanovic, S.; Szpunar, J.A. Enhancement of biocompatibility of 316LVM stainless steel by cyclic potentiodynamic passivation. *J. Biomed. Mater. Res. Part A* **2009**, *89A*, 1049–1062. [CrossRef]
144. Wang, X.; Liu, Z.; Chen, Y.; Sun, J.; He, Q.; Liu, Q.; Liu, G.; Xie, K. Abrasive resistance and corrosion properties of AISI 316 sieve via low-temperature gaseous nitriding. *Surf. Coat. Technol.* **2019**, *361*, 349–356. [CrossRef]
145. Abreu, C.M.; Cristóbal, M.J.; Merino, P.; Nóvoa, X.R.; Pena, G.; Pérez, M.C. Electrochemical behaviour of an AISI 304L stainless steel implanted with nitrogen. *Electrochim. Acta* **2008**, *53*, 6000–6007. [CrossRef]
146. Hirschorn, B.; Orazem, M.E.; Tribollet, B.; Vivier, V.; Frateur, I.; Musiani, M. Constant-Phase-Element Behavior Caused by Resistivity Distributions in Films. *J. Electrochem. Soc.* **2010**, *157*, C458–C463. [CrossRef]
147. Jüttner, K. Electrochemical impedance spectroscopy (EIS) of corrosion processes on inhomogeneous surfaces. *Electrochim. Acta* **1990**, *35*, 1501–1508. [CrossRef]
148. Bai, H.; Wang, F. Protective Properties of High Temperature Oxide Films on Ni-based Superalloys in 3.5% NaCl Solution. *J. Mater. Sci. Technol.* **2007**, *23*, 541–546.
149. Luiz, L.A.; Kurelo, B.C.E.S.; Souza, G.B.; Andrade, J.; Marino, C.E.B. Effect of nitrogen plasma immersion ion implantation on the corrosion protection mechanisms of different stainless steels. *Mater. Today Commun.* **2021**, *28*, 102655. [CrossRef]
150. Fossati, A.; Borgioli, F.; Galvanetto, E.; Bacci, T. Corrosion resistance properties of glow-discharge nitrided AISI 316L austenitic stainless steel in NaCl solutions. *Corros. Sci.* **2006**, *48*, 1513–1527. [CrossRef]
151. Örnek, C.; Leygraf, C.; Pan, J. Passive film characterisation of duplex stainless steel using scanning Kelvin probe force microscopy in combination with electrochemical measurements. *NPJ Mater. Degrad.* **2019**, *3*, 8. [CrossRef]
152. Rybalka, K.V.; Shaldaev, V.S.; Beketaeva, L.A.; Malofeeva, A.N.; Davydov, A.D. Development of pitting corrosion of stainless steel 403 in sodium chloride solutions. *Russ. J. Electrochem.* **2010**, *46*, 196–204. [CrossRef]
153. Jin, S.; Atrens, A. Passive films on stainless steels in aqueous media. *Appl. Phys. A Solids Surf.* **1990**, *50*, 287–300. [CrossRef]
154. Schibicheski Kurelo, B.C.E.; de Souza, G.B.; Serbena, F.C.; Lepienski, C.M.; Chuproski, R.F.; Borges, P.C. Improved saline corrosion and hydrogen embrittlement resistances of superaustenitic stainless steel by PIII nitriding. *J. Mater. Res. Technol.* **2022**, *18*, 1717–1731. [CrossRef]
155. Olzon-Dionysio, M.; Olzon-Dionysio, D.; Campos, M.; Shigeyosi, W.T.; de Souza, S.D.; de Souza, S. Corrosion resistance of AISI 316L plasma nitrided at different temperatures and times. *Hyperfine Interact.* **2019**, *240*, 26. [CrossRef]
156. Lei, M.K.; Zhu, X.M. Plasma-based low-energy ion implantation of austenitic stainless steel for improvement in wear and corrosion resistance. *Surf. Coat. Technol.* **2005**, *193*, 22–28. [CrossRef]
157. Kamachi Mudali, U.; Shankar, P.; Ningshen, S.; Dayal, R.K.; Khatak, H.S.; Raj, B. On the pitting corrosion resistance of nitrogen alloyed cold worked austenitic stainless steels. *Corros. Sci.* **2002**, *44*, 2183–2198. [CrossRef]
158. Lei, M.K.; Zhang, Z.L.; Zhu, X.M. Effects of nitrogen-induced hcp martensite formation on corrosion resistance of plasma source ion nitrided austenitic stainless steel. *J. Mater. Sci. Lett.* **1999**, *18*, 1537–1538. [CrossRef]
159. Chao, K.L.; Liao, H.Y.; Shyue, J.J.; Lian, S.S. Corrosion behavior of high nitrogen nickel-free Fe-16Cr-Mn-Mo-N stainless steels. *Metall. Mater. Trans. B Process Metall. Mater. Process. Sci.* **2014**, *45*, 381–391. [CrossRef]
160. Escalada, L.; Dalibon, E.L.; Brühl, S.P.; Manova, D.; Mändl, S.; Simison, S. Influence of Inclusions in the Corrosion Behavior of Plasma Nitrided Stainless Steel. *Adv. Eng. Mater.* **2022**, 2201112. [CrossRef]
161. Saravanan, P.; Raja, V.S.; Mukherjee, S. Effect of alloyed molybdenum on corrosion behavior of plasma immersion nitrogen ion implanted austenitic stainless steel. *Corros. Sci.* **2013**, *74*, 106–115. [CrossRef]
162. Burstein, G.T.; Vines, S.P. Repetitive Nucleation of Corrosion Pits on Stainless Steel and the Effects of Surface Roughness. *J. Electrochem. Soc.* **2001**, *148*, 504–516. [CrossRef]
163. Li, N.; Wang, N. The effect of duplex Surface mechanical attrition and nitriding treatment on corrosion resistance of stainless steel 316L. *Sci. Rep.* **2018**, *8*, 8454. [CrossRef]

164. Picard, S.; Memet, J.B.; Sabot, R.; Grosseau-Poussard, J.L.; Rivière, J.P.; Meilland, R. Corrosion behaviour, microhardness and surface characterisation of low energy, high current ion implanted austenitic stainless steel. *Mater. Sci. Eng. A* **2001**, *303*, 163–172. [CrossRef]
165. Frangini, S.; De Cristofaro, N. Analysis of the galvanostatic polarization method for determining reliable pitting potentials on stainless steels in crevice-free conditions. *Corros. Sci.* **2003**, *45*, 2769–2786. [CrossRef]
166. Spies, H.-J.; Eckstein, C.; Biermann, H.; Franke, A. Corrosion behaviour of stainless steels after low temperature thermochemical treatment. *Materwiss. Werksttech.* **2010**, *41*, 133–141. [CrossRef]
167. Sun, Y. Enhancement in corrosion resistance of austenitic stainless steels by surface alloying with nitrogen and carbon. *Mater. Lett.* **2005**, *59*, 3410–3413. [CrossRef]
168. Borowski, T. Enhancing the Corrosion Resistance of Austenitic Steel Using Active Screen Plasma Nitriding and Nitrocarburising. *Materials* **2021**, *14*, 3320. [CrossRef]
169. Martinesi, M.; Bruni, S.; Stio, M.; Treves, C.; Bacci, T.; Borgioli, F. Biocompatibility evaluation of surface-treated AISI 316L austenitic stainless steel in human cell cultures. *J. Biomed. Mater. Res. Part A* **2007**, *80*, 131–145. [CrossRef]
170. Martinesi, M.; Stio, M.; Treves, C.; Borgioli, F. Biocompatibility studies of low temperature nitrided and collagen-I coated AISI 316L austenitic stainless steel. *J. Mater. Sci. Mater. Med.* **2013**, *24*, 1501–1513. [CrossRef] [PubMed]
171. Stio, M.; Martinesi, M.; Treves, C.; Borgioli, F. In vitro response of human peripheral blood mononuclear cells to AISI 316L austenitic stainless steel subjected to nitriding and collagen coating treatments. *J. Mater. Sci. Mater. Med.* **2015**, *26*, 100. [CrossRef] [PubMed]
172. Stio, M.; Martinesi, M.; Treves, C.; Borgioli, F. Cultures and co-cultures of human blood mononuclear cells and endothelial cells for the biocompatibility assessment of surface modified AISI 316L austenitic stainless steel. *Mater. Sci. Eng. C* **2016**, *69*, 1081–1091. [CrossRef]
173. Valero Vidal, C.; Igual Muñoz, A. Electrochemical characterisation of biomedical alloys for surgical implants in simulated body fluids. *Corros. Sci.* **2008**, *50*, 1954–1961. [CrossRef]
174. Lei, M.K.; Zhu, X.M. In vitro corrosion resistance of plasma source ion nitrided austenitic stainless steels. *Biomaterials* **2001**, *22*, 641–647. [CrossRef]
175. Yazıcı, M.; Çomaklı, O.; Yetim, T.; Yetim, A.F.; Çelik, A. The effect of plasma nitriding temperature on the electrochemical and semiconducting properties of thin passive films formed on 316L stainless steel implant material in SBF solution. *Surf. Coat. Technol.* **2015**, *261*, 181–188. [CrossRef]
176. Dashtbozorg, B.; Li, X.; Romano, J.; Garcia–Giron, A.; Sammons, R.L.; Dimov, S.; Dong, H. A study on the effect of ultrashort pulsed laser texturing on the microstructure and properties of metastable S phase layer formed on AISI 316L surfaces. *Appl. Surf. Sci.* **2020**, *511*, 145557. [CrossRef]
177. Flis, J.; Kuczynska, M. Effect of Low-Temperature Plasma Nitriding on Corrosion of 304L Stainless Steel in Sulfate and Chloride Solutions. *J. Electrochem. Soc.* **2004**, *151*, B573–B580. [CrossRef]
178. Buhagiar, J.; Dong, H. Corrosion properties of S-phase layers formed on medical grade austenitic stainless steel. *J. Mater. Sci. Mater. Med.* **2012**, *23*, 271–281. [CrossRef] [PubMed]
179. Buhagiar, J.; Spiteri, A.; Sacco, M.; Sinagra, E.; Dong, H. Augmentation of crevice corrosion resistance of medical grade 316LVM stainless steel by plasma carburising. *Corros. Sci.* **2012**, *59*, 169–178. [CrossRef]
180. Li, C.X.; Bell, T. Corrosion properties of active screen plasma nitrided 316 austenitic stainless steel. *Corros. Sci.* **2004**, *46*, 1527–1547. [CrossRef]
181. Sun, Y. Response of cast austenitic stainless steel to low temperature plasma carburizing. *Mater. Des.* **2009**, *30*, 1377–1380. [CrossRef]
182. Ceschini, L.; Chiavari, C.; Lanzoni, E.; Martini, C. Low-temperature carburised AISI 316L austenitic stainless steel: Wear and corrosion behaviour. *Mater. Des.* **2012**, *38*, 154–160. [CrossRef]
183. Lin, K.; Li, X.; Sun, Y.; Luo, X.; Dong, H. Active screen plasma nitriding of 316 stainless steel for the application of bipolar plates in proton exchange membrane fuel cells. *Int. J. Hydrog. Energy* **2014**, *39*, 21470–21479. [CrossRef]
184. Tian, R.; Sun, J.; Wang, L. Plasma-nitrided austenitic stainless steel 316L as bipolar plate for PEMFC. *Int. J. Hydrog. Energy* **2006**, *31*, 1874–1878. [CrossRef]
185. Tandon, V.; Patil, A.P.; Rathod, R.C. Influence of Time on Low Temperature Salt Bath Nitriding and its Corrosion Behavior of 316L ASS in PEMFC Environment. *Prot. Met. Phys. Chem. Surf.* **2020**, *56*, 772–779. [CrossRef]
186. Spies, H.-J.; Eckstein, C.; Zimdars, H. Structure and corrosion behaviour of stainless steels after plasma and gas nitriding. *Surf. Eng.* **2002**, *18*, 459–460. [CrossRef]
187. Flis, J.; Gajek, A. Impedance parameters of nitrided 304L stainless steel in an acidified sulphate solution. *J. Electroanal. Chem.* **2001**, *515*, 82–90. [CrossRef]
188. Kuczynska-Wydorska, M.; Flis, J. Corrosion and passivation of low-temperature nitrided AISI 304L and 316L stainless steels in acidified sodium sulphate solution. *Corros. Sci.* **2008**, *50*, 523–533. [CrossRef]
189. Sun, Y. Depth-profiling electrochemical measurements of low temperature plasma carburised 316L stainless steel in 1M H_2SO_4 solution. *Surf. Coat. Technol.* **2010**, *204*, 2789–2796. [CrossRef]

190. Corujeira Gallo, S.; Dong, H. Corrosion behaviour of direct current and active screen plasma carburised AISI 316 stainless steel in boiling sulphuric acid solutions. *Corros. Eng. Sci. Technol.* **2011**, *46*, 8–16. [CrossRef]
191. Sun, Y.; Bailey, R. Comparison of Wear Performance of Low Temperature Nitrided and Carburized 316L Stainless Steel under Dry Sliding and Corrosive-Wear Conditions. *J. Mater. Eng. Perform.* **2023**, *32*, 1238–1247. [CrossRef]